Global signatures of the human mesenchymal stromal cell secretome: A comparative proteomic analysis of iPSC and tissue-derived MSC secretomes before and after inflammatory licensing

Margeaux Hodgson-Garms
Monash University; Cynata Therapeutics
Matthew Moore
Monash University
Mikaël Martino
EMBL Australia, Monash University https://orcid.org/0000-0002-5012-4605
Kilian Kelly
Cynata Therepeutics
Jessica Frith
jessica.frith@monash.edu

Monash University https://orcid.org/0000-0002-6558-5412

Article

Keywords: Mesenchymal stromal cell, MSC, secretome, proteomics, inflammatory licensing, iMSC

Posted Date: April 5th, 2024

DOI: https://doi.org/10.21203/rs.3.rs-4054317/v1

Additional Declarations: There is a conflict of interest The authors declare the following competing interests: K.K is an employee and shareholder of Cynata Therapeutics. The authors declare that this study received funding from Cynata Therapeutics. The funder was not involved in the study design, collection, analysis, interpretation of data, the writing of this article or the decision to submit it for publication, outside of the contributions of author K.K.

Abstract

Multipotent mesenchymal stromal cells (MSCs) are one of the most heavily studied cell therapies worldwide, with much of their therapeutic potential underpinned by their complex secretory profiles. Like MSCs themselves, their secretome varies significantly between donors, sources, and according to microenvironmental cues. As such, there remains a lack of consensus as to the global nature of the MSC secretome, its source-based heterogeneity, and the dynamic changes it undergoes in response to inflammatory licensing. A full understanding of these differences is essential in understanding the mechanisms that drive MSC-based tissue repair and in optimising the properties of MSCs for cell therapies.

This study used liquid chromatography tandem mass spectrometry (LC/MS-MS) to characterise and compare the secretomes of 13 MSC lines, sourced from bone marrow (BM.MSCs), umbilical cord (UC.MSCs), and adipose tissue (AT.MSCs), alongside multiple batches of clinical and commercial grade induced pluripotent stem cell derived MSCs (iMSCs), all under both resting and inflammatory licensed conditions. We confirm, for the first time, that iMSCs successfully recapitulate the process of inflammatory licensing, validating their comparability to tissue-derived MSCs and providing important support for their application as an immunotherapy. We identify a global and dichotomous signature of the MSC secretome and inflammatory licensing, where resting secretomes are defined by prominent extracellular matrix (ECM) proteins and overrepresentation of pro-regenerative and wound healing processes, while licensed secretomes downregulate these factors in favour of chemotactic and immunosuppressive proteins and immunomodulatory processes. Furthermore, under both resting and licensed conditions, MSC secretomes separate based on source, with iMSC and UC.MSC secretomes more similar to each other, containing higher concentrations of proteins indicating proliferative potential and telomere maintenance, while adult tissue-derived, BM.MSC and AT.MSC secretomes contained more fibrotic and ECM proteins

This dataset provides a detailed atlas of resting and licensed MSC secretomes and generates insights into the molecular mechanisms underlying the differences observed between MSC secretomes from different sources or functional states. Going forward, this will inform the design of more effective MSC-based therapies by identifying the most suitable MSC source for a particular application, and allow the development of tailored culture conditions and/or preconditioning methods to enhance the therapeutic potential of these cells, potentially identifying specific factors that can be adapted for pharmaceutical intervention.

1 Introduction

Mesenchymal stromal cells (MSCs) are a heterogeneous population of multipotent cells that can be isolated from virtually all organs and tissues[1] or generated from induced pluripotent stem cells (iMSCs)[2]. They are broadly defined by the International Society for Cell and Gene Therapy (ISCT) as plastic adherent stromal cells; expressing CD73, CD90, and CD105 surface antigens in the absence of CD34,

CD45, CD14, CD19, and HLA-DR; and with the capacity to differentiate along osteogenic, chondrogenic, and adipogenic linages *in vitro*[3]. Beyond this MSCs also possess significant immunomodulatory capacity and have been widely documented to aid in tissue regeneration and repair[4,5]. This has led to MSCs becoming one of the most heavily studied cell therapies worldwide. To fully realise their clinical potential, however, fundamental aspects of MSC biology and how exactly they exert their immunomodulatory and pro-regenerative functions, must be clarified. This is complicated by the dynamic nature of MSCs and the heterogeneity that they exhibit between tissue sources, donors, and within individual populations[6].

The range of clinical indications to which MSCs are applied is incredibly diverse, but typically targets two pathophysiological categories: immune and inflammatory conditions, such as graft-versus-host disease[7] and Crohn's disease; or tissue repair and regeneration applications, including soft tissue wound healing[8] and cardiac repair[9]. The breadth of these applications is driven by the fact that MSCs exhibit several distinct phenotypes, between which they switch in response to microenvironmental cues, a quality referred to as plasticity[10,11]. The current model of MSC plasticity, describes three unique phenotypes; resting MSCs, which are thought to be responsible for maintaining the haematopoietic niche and stromal tissues *in vivo*; a pro-inflammatory phenotype, referred to as MSC1, and an immuno-suppressive phenotype, referred to as MSC2[12–16]. This nomenclature mirrors the system applied to the M1/M2 polarisation of macrophages, reflecting similar engagement throughout the wound healing process. This model of MSC plasticity postulates that early tissue-injury signals result in pro-inflammatory MSC1 licensing, causing MSCs to home to the site of an injury, recruit peripheral immune cells, and participate in the early phases of wound healing. Subsequent anti-inflammatory licensing to an MSC2 phenotype successively aids in resolution of the immune response and wound healing process[17–19].

Whilst MSCs were originally predicted to repair injured tissues through engraftment and subsequent differentiation[20–22], most studies in which MSCs have been administered lack evidence of long-term cell survival, despite showing functional improvements [22–25]. Indeed, up to 95% of systemically administered MSCs are cleared from the bloodstream in less than five minutes[26–28] and repair of injured tissues is often observed too rapidly to be explained by direct differentiation of administered MSCs[29]. As such, the therapeutic potential of MSCs is now strongly attributed to their secretion of bioactive and paracrine factors, which are known to change rapidly, reflecting their phenotypic plasticity[23,30–37].

The MSC secretome consists of a complex milieu of biologically active factors, including extracellular vesicles, chemokines and receptors (CCL2 ,CCL5, CXCL8-11), mitogenic and angiogenic growth factors (FGF, VEGF, TGF-β), inflammatory cytokines (IL-6, IL-8), immunomodulatory factors (indoleamine 2,3-dioxygenase (IDO), MHC-I, MCH-II), and extracellular matrix (ECM) components (collagens, fibronectins, integrins)[38–42]. While the roles that individual factors play in driving the clinically relevant functions of the MSC secretome are regularly subject to review[32,43,44], there remains little consensus on the complete MSC secretory profile, suggesting that a more comprehensive understanding is still required to effectively capitalise on their therapeutic potential. Importantly, how the MSC secretome changes with different phenotypes has also not previously been described in detail. This is of particular importance as many of

the targeted applications of MSCs involve delivery of live and responsive cells into a dynamic *in vivo* microenvironment.

Of the three established MSC phenotypes, resting and MSC2 are of the greatest clinical interest as it is these phenotypes that likely drive the potential of MSCs as pro-regenerative and immunosuppressive agents[12,14]. Despite this, inflammatory licensing is often overlooked in comparative and functional studies of MSCs, and little is yet known of how the secretome changes with this process. Importantly, as with other aspects of MSC identity, the MSC secretome differs between donors and between tissue sources[32,45] and there is a lack of consensus as to how the tissue specific identity of MSCs affects their inflammatory response and plasticity. This constitutes a significant gap in our understanding that impacts the ability to effectively select optimal MSC lines for specific applications. Furthermore, the secretome of iMSCs has yet to be fully characterised under either resting or inflammatory licensed conditions.

This study addressed these questions by using high resolution two-dimensional liquid chromatography tandem mass spectrometry (LC-MS/MS) to profile the secretome of MSCs under both resting and MSC2 inflammatory licensed conditions. To address the heterogeneity that exists between MSC tissue-sources and donors, as well as the lack of information on the secretome of iMSCs, this study profiled multiple batches of clinical and commercial-grade iPSC-derived MSCs, in parallel with multiple tissue-derived MSCs, sourced from triplicate donors of bone marrow, adipose tissue, and umbilical cord. This generated a comprehensive atlas of the MSC secretome, allowing identification of a conserved profile of MSC2 inflammatory licensing, and a robust comparison of resting and MSC2 secretomes. The data allows the comparison of iPSC and tissue-derived MSC secretomes and provides the first evidence that iMSCs are capable of comparable inflammatory licensing. Additionally, comparisons may be drawn between the secretomes of either resting or licensed MSCs derived from adult versus natal tissue sources, including umbilical cord, adipose tissue, and bone marrow; between clinical and commercial grade iMSCs; and between individual donors or batches of each MSC population. This data set will also serve as a framework to predict the therapeutic potential of different MSCs, identifying the MSC source most likely to have optimal therapeutic effects for each of the varying target applications.

2 Results

To compare the immune plasticity and secretory profiles of iPSC and tissue-derived MSCs a panel of 13 MSC lines was established. This consisted of three donors each of bone marrow (BM.MSCs 1–3), adipose tissue (AT.MSCs 1–3), and umbilical cord (UC.MSCs 1–3)-derived MSCs, three batches of Cynata Therapeutics' CYP001™ clinical iMSCs (CYN.iMSCs 1–3), and one batch of commercially available iMSCs (Cellular Dynamics Incorporated) (CDI.iMSC 4). This panel allowed comparisons between iPSC and tissue-derived MSCs, between MSCs from different tissue sources (including both adult and natal tissues), and between MSCs from different batches/donors of the same source **(Tab. S1)**. The basic characteristics of the MSC lines were assessed to confirm compliance with the ISCT minimal criteria. All MSC lines successfully adhered to, and proliferated on, tissue-culture plastic. They expressed CD73,

CD90, and CD105 surface markers in the absence of CD14, CD19, CD34, CD45, and HLA-DR **(Fig. S1)**, and demonstrated the ability to differentiate *in vitro* along the osteogenic, adipogenic and chondrogenic lineages **(Fig. S2)**.

Inflammatory licencing of MSCs

Previous studies have shown that MSC licensing can be initiated via stimulation with inflammatory cytokines, where short exposure times and lower concentrations result in an MSC1 phenotype, while higher concentrations or extended exposure result in an MSC2 phenotype[46–49] **(**Fig. 1a**)**. Here, an MSC2 phenotype was induced by 48 h. exposure to 15 ng/ml IFNγ and 15 ng/ml TNFα as per the ISCT recommendations on immune functional assays for MSCs[50]. Successful MSC2 licencing was validated by measuring the upregulation of HLA-ABC and HLA-DR surface markers and the secretion of IDO[11,12,50] **(**Fig. 1b**)**.

Upon exposure to the inflammatory cytokines, there were obvious changes to cell morphology, with visible membrane ruffling and reshaping of the cytoplasm **(**Fig. 1c**)**. To validate that these changes were characteristic of inflammatory licensing, the expression of HLA-ABC and HLA-DR surface markers was measured using flow cytometry, both with and without cytokine exposure. In the absence of inflammatory cytokines (resting MSC state), all lines maintained an HLA-DR^{neg} phenotype, while the proportion of cells expressing HLA-ABC varied between MSC source. The percentage of HLA-ABC^{pos} cells in resting MSC lines was lowest in iMSCs (1.5–14%), followed by UC.MSCs (17–66%), and AT.MSCs (38–45%), and highest in BM.MSCs (50–80%) **(**Fig. 1d**)**. In contrast, after exposure to inflammatory cytokines, > 98% of MSCs expressed both HLA-DR and HLA-ABC, confirming that all the MSC populations had responded to the licencing procedure (licensed MSC state).

To subsequently determine whether the licenced MSCs had acquired an MSC1 or MSC2 phenotype, the level of IDO in MSC conditioned medium (CM) was assessed by ELISA. IDO plays a major role in the immunosuppressive functions that define the anti-inflammatory MSC2 phenotype, and separate it from the MSC1 phenotype[11,12]. Exposure to inflammatory cytokines increased IDO levels in MSC CM by more than 10-fold for all MSC lines, indicating acquisition of an MSC2 phenotype. Importantly, while CM was produced from a standardised 1x10^4 cells/mL of media, the concentrations of IDO varied considerably between sources. iMSCs secreted the most IDO (15.5–18 ng/mL), followed by UC.MSCs (2.5-4 ng/mL) and AT.MSCs (1.2–3.5 ng/ mL), with BM.MSCs producing the least (0.5–0.7 ng/mL) **(**Fig. 1e**)**. Collectively, this indicated successful licencing of all MSCs lines after 48 h exposure to 15 ng/ml IFNγ and 15 ng/ml TNFα, with a specific shift from a resting to MSC2 phenotype. These populations will subsequently be referred to as resting and licensed MSCs, respectively.

Harvest of CM and quality assessment of MSC secretomes

To produce a comprehensive, unbiased proteomic profile of the MSC secretome, CM was harvested from both resting and licensed MSCs and LC-MS/MS was used to detect and quantify proteins. After stringent

quality control to remove contaminents and media components, total protein lists were filtered against gene ontology cellular compartment (CC) term: *extracellular space* (GO:0005615) to identify secreted proteins. Total and extracellular protein lists are provided in **Supplementary material A**.

A total of 504 secreted proteins were identified in resting CM across all MSC lines, with 746 proteins identified in licensed CM. Of these, 39 proteins (5%) were unique to resting conditions, 281 (35.8%) were unique to licensed conditions, with the remaining 465 (59.2%) detected in both resting and licensed CM (Fig. 2a). Interestingly, a greater number of distinct proteins were identified in CM from iMSCs as compared to MSCs from other sources, regardless of whether the cells were in a resting or licensed state (**Fig. S4).** Mapping of the secreted proteins to gene ontology biological process (BP) terms indicated that most of the proteins were linked to '*biological regulation*', '*response to stimulus*', and '*metabolic processes*', with significant number of proteins involved in '*regulation of gene expression*', '*general signalling'* and '*cell communication*', regardless of whether they were present in resting or licenced CM (Fig. 2b)**.** This emphasises the highly regulatory role that MSCs play under both resting and licensed conditions.

There were substantial differences between the MSC secretomes, evidenced by varying patterns of protein intensity when comparing i) resting and licensed MSCs, ii) iMSCs and tissue-derived MSCs, and iii) MSCs from different tissue sources (Fig. 2c). Principal component analysis (PCA) was used to investigate the clustering and similarity of the MSC secretomes and showed clear effects of both inflammatory licencing and MSC source (Fig. 2d). Individual donors/batches from each combination of MSC source and treatment type clustered together, but there was distinct separation of the samples from different MSC sources and between those collected from cells in resting or licenced conditions. Principal component one (PC1) accounted for 40% of the variation and largely corresponded to differences due to MSC source. The greatest separation was observed between iMSC and tissue-derived MSC secretomes in general, with UC.MSC secretomes also separating from BM.MSC and AT.MSC secretomes along PC1, indicating greater similarity between the secretomes of iMSC and natal MSCs than between iMSC and adult tissue-derived MSCs. Principle component two (PC2) accounted for 14% of the variation of MSC secretomes and corresponded to separation of resting and licensed secretomes, which clearly formed into two distinct clusters.

A conserved proteomic signature of licensed MSCs

The changes that MSCs undergo with inflammatory licensing, and the affect that this has on their secretome, represent a crucial gap in our understanding of MSC behaviour. To identify a conserved signature of inflammatory licensing in the MSC secretome, proteins that were differentially expressed (DE) in all paired resting-licenced MSC lines were identified. This detected 43 proteins that were differentially expressed between resting and licensed secretomes, regardless of MSC source or donor. Of these, 32 proteins were upregulated in licensed secretomes, with the remaining 11 upregulated in resting secretomes (Fig. 3a)**.** Differential expression of all secreted proteins is provided in **Suplementary material A**.

DE proteins included known drivers of key MSC capabilities, such as IDO, prostaglandin E-synthase (PTGES3), TNFα stimulated gene-6 (TSG-6), monocyte chemoattractant protein 1 (CCL2), interleukin 6 (IL6), Cathepsin S (CTSS), and HLA-A, B, and C[43]. This underscores the considerable influence that licensing of MSCs will play on their functional capacity. Additionally, proteins not previously linked to inflammatory licencing were also identified as DE, including laminin Subunit Alpha 2 (LAMA2), aldolase B (ALDOB) and midkine (MDK) (Fig. 3b). These DE proteins represent a conserved signature of the secretome of resting and licensed MSCs, which can provide important fundamental insights into the nature of the different MSC states and their functional differences.

To verify which proteins were the main drivers of the separation of resting and licensed secretomes (PC2), PCA loadings were calculated (Fig. 3c). These showed that the principal component separating resting and licensed MSC secretomes was primarily driven by five proteins; chemokine (C-X-C motif) ligand 9 (CXCL9), CXCL10, CXCL11, chemokine (C-C motif) ligand 5 (CCL5) and interleukin-18 binding protein (IL18BP), all of which were upregulated by over 20-fold in the licenced secretomes. Proteins that were more abundant in the resting MSC secretome included collagens (COL)1A1, COL1A2, COL2A1, microfibril-associated glycoprotein 4 (MFAP4), prostaglandin F2 receptor negative regulator (PTGFRN), thrombospondin-2 (THBS2), and syndecan-binding protein (SDCBP). Significantly DE proteins between paired resting-licensed secretomes in included in **(Tab. S2)**.

To better understand the relationships between key proteins, the STRING database[51] was used to generate interaction networks between proteins upregulated in resting or in licensed secretomes (Fig. 3d). This identified highly interconnected networks, with relatively few disconnected proteins, for each the resting and licensed secretomes, suggesting strong functional overlap within resting and licensed secretory profiles. To explore this, and the biological impact of secretory profile changes, DE proteins were interrogated for statistically over-represented BP using GO-term enrichment analysis. When analysing the most significant processes, those with the lowest false discovery rate (FDR), it emerged that proteins enriched in resting secretomes were overrepresented in processes linked to extracellular matrix deposition and remodelling, including '*collagen fibril organisation*' (90-fold), '*extracellular matrix organization*' (24.7-fold), '*bone morphogenesis*' (52.1-fold), '*skin morphogenesis*' (219.3-fold), '*replacement ossification*' (121-fold), '*skeletal system development*' (12.5-fold), '*cartilage development*' (24.8-fold), '*circulatory system development*' (7.6-fold) and *'response to TGFβ'* (19.4-fold) (Fig. 3e). In contrast, proteins enriched in the licensed MSC secretomes were predominantly linked to processes involved in immune regulation, including '*immune system process*' (4.5-fold), '*immune response*' (5.8-fold), '*positive regulation of immune system process*' (8.1-fold), '*humoral immune response*' (18-fold), '*adaptive immune response*' (9.3-fold), and '*complement activation*' (35.9-fold) (Fig. 3f) (Table 1). This emphasises the pro-regenerative properties of the resting MSC secretome in contrast to the immunomodulatory properties of the MSC2 secretome. Moreover, it suggests that the pro-regenerative properties of the resting MSC secretome are heavily downregulated with inflammatory licensing.

Table 1
Top biological process terms overrepresented amongst DE proteins upregulated in either resting or licensed MSC secretomes.

Group	*Biological process*	*Fold enrichment*	*FDR*
Overrepresented in licensed	Immune system process	4.55	3.69E-10
	Immune response	5.78	3.69E-10
	Positive regulation of immune system process	8.08	2.90E-08
	Regulation of immune system process	5.91	8.81E-08
	Humoral immune response	17.97	2.79E-07
	Biological process involved in interspecies interaction between organisms	5.35	2.79E-07
	Response to biotic stimulus	5.45	7.45E-07
	Regulation of immune response	7.44	8.95E-07
	Response to external biotic stimulus	5.23	3.64E-06
	Response to other organism	5.23	3.64E-06
	Positive regulation of apoptotic cell clearance	120.61	4.10E-06
	Regulation of apoptotic cell clearance	109.65	5.66E-06
	Adaptive immune response	9.35	6.31E-06
	Positive regulation of immune response	9.00	8.36E-06
	Defense response	4.45	1.93E-05
	Response to molecule of bacterial origin	12.06	1.94E-05
	Complement activation	35.90	2.04E-05

Group	*Biological process*	*Fold enrichment*	*FDR*
	Response to bacterium	7.81	2.08E-05
	T cell migration	35.06	2.08E-05
	Innate immune response	6.02	5.40E-05
	Chemokine-mediated signaling pathway	28.45	5.40E-05
	Response to chemokine	26.22	7.14E-05
	Cellular response to chemokine	26.22	7.14E-05
	Neutrophil chemotaxis	24.51	9.25E-05
	Response to lipopolysaccharide	11.23	1.13E-04
Overrepresented in resting	Collagen fibril organization	89.97	4.84E-05
	Extracellular matrix organization	24.71	9.24E-05
	Collagen metabolic process	64.38	9.24E-05
	Extracellular structure organization	24.64	9.24E-05
	External encapsulating structure organization	24.43	9.24E-05
	Cartilage development involved in endochondral bone morphogenesis	159.49	9.24E-05
	Endochondral bone morphogenesis	89.20	3.82E-04
	Bone morphogenesis	52.11	1.69E-03
	Skin morphogenesis	219.30	2.38E-03
	Supramolecular fiber organization	9.93	4.41E-03

Group	*Biological process*	*Fold enrichment*	*FDR*
	Endochondral ossification	120.99	6.02E-03
	Replacement ossification	120.99	6.02E-03
	Skeletal system development	12.49	8.76E-03
	Cartilage development	24.83	8.76E-03
	Anatomical structure morphogenesis	4.28	1.00E-02
	Collagen biosynthetic process	76.28	1.00E-02
	Skeletal system morphogenesis	22.49	1.00E-02
	Bone development	21.39	1.00E-02
	Circulatory system development	7.63	1.00E-02
	Positive regulation of epithelial to mesenchymal transition	67.48	1.03E-02
	Cellular response to transforming growth factor beta stimulus	19.86	1.03E-02
	Response to transforming growth factor beta	19.42	1.05E-02
	Connective tissue development	18.60	1.10E-02
	Blood vessel development	9.56	1.20E-02
	Vasculature development	9.17	1.35E-02
	Cellular response to amino acid stimulus	46.17	1.66E-02

To better understand the regulatory mechanisms that drive the differences between resting and licensed MSC phenotypes, DE protein lists were further queried for overrepresentation in specific transcription factor (TF) regulatory networks using the hTFtarget database[52]. Regulatory networks governing the expression of proteins upregulated in resting MSC secretomes were enriched for TFs involved in

developmental processes, including SP3 (32.8-fold), KLF13 (442.7-fold), and SOX4 (885.4-fold). In contrast, regulatory networks governing expression of proteins upregulated in licensed MSC secretomes were enriched for known drivers of immune responses, including STAT1 (7.8-fold), STAT2 (7.0-fold), REL (10.8-fold), RELA (7.8-fold), RELB (23.9-fold), NFkB1 (5.6-fold) and NFkB2 (9.9-fold) targets, as well as IRF1 (8.7-fold), IRF3 (82.5-fold), and CEBPD (45.3-fold) **(Table 2)**. This suggests that the resting MSC phenotype is maintained by activity of a limited number of TFs which play important roles in regulating developmental processes and tissue homeostasis while the change in secretory profiles with inflammatory licensing is driven by activation of IRF and Rel family TFs, which are known regulators of inflammatory processes[53–57].

Table 1
Overrepresented transcription factor target regulatory networks of proteins enriched in licensed MSC secretomes.

	TF regulatory networks	Fold enrichment	Adjusted P values
Overrepresented in resting	SP3	32.8	2.63E-2
	KLF13	442.7	2.63E-2
	SOX4	885.4	2.63E-2
Overrepresented in licensed	STAT1	7.8	1.60E-5
	IRF3	82.5	2.89E-4
	RELA	7.8	4.12E-4
	RELB	23.9	4.12E-4
	NFKB2	9.9	4.12E-4
	REL	10.8	1.25E-3
	NFKB1	5.6	1.92E-3
	STAT2	7.0	1.92E-3
	CEBPD	45.3	9.22E-3
	IRF1	8.7	9.68E-3

Overall, these data provide a conserved signature of the MSC secretome in resting and MSC2 states. Key changes between these suggest that the role of resting MSCs focuses heavily on tissue maintenance and repair, through the deposition of ECM proteins and the promotion of developmental and morphogenic processes. In contrast, under inflammatory licensed conditions, these functions are strongly downregulated, in favour of the secretion of a complex milieu of immunomodulatory proteins.

Differences in the secretome of MSCs by cell source

While clear differences between the secretomes of resting and licensed MSCs showed the impact of inflammatory licencing (PC2,14.1% of variation), significantly more of the variation between the secretomes was due to the MSC source (PC1, 40.0% of variation). While most of these differences were specific to either resting or licensed MSCs, it is noteworthy that a small subset of proteins drove the separation of all MSC sources along PC1 regardless of whether the cells were in a resting or licensed state. These were profilin-2 (PFN2), eukaryotic translation initiation factor 2 subunit 1 (EIF2S1), and high mobility group box 1 (HMGB1), which were highest in iMSC secretomes and lowest in BM.MSC and AT.MSC secretomes **(Fig. S5a-c)**. Conversely, cystatin-2 (CST2) and proenkephalin (PENK) were enriched in adult tissue-derived MSCs and lowest in iMSCs **(Fig. S5d-e)**. Expression of these proteins likely represents a singular conserved variable driving source-based heterogeneity of MSCs regardless of functional state.

Within the resting secretomes, 387 proteins (59.2%) were conserved between all MSC sources. The iMSC secretomes were most different of all the samples and contained 91 unique proteins, while the UC.MSC and AD.MSC secretomes each contained just 7 unique proteins, and the BM.MSC secretomes 2 unique proteins **(**Fig. 4a**)**. Using the coefficient of variation (CoV) to indicate the homogeneity of the secretomes within each source, it was evident that there was less variability between different iMSC batches (CoV 18%) than between different donors of BM.MSCs (CoV 41%), UC.MSCs (CoV 26%) or AT.MSCs (CoV 24%) **(Fig. S6a)**. PCA was used to visualise the overall similarity between the secretomes and showed that separate donors/batches of MSCs from the same source clustered together, while different sources were separated. The MSC secretomes separated by source along PC1 (45% of overall variation) with BM.MSCs plotting on the most positive end of PC1, followed by AT.MSCs, UC.MSC, and finally iMSCs, which plotted at the most negative end **(**Fig. 4b**)**. This axis of separation, with iMSC and UC.MSC secretomes on one end and adult-tissue derived secretomes on the other end, was driven by CD155 (poliovirus receptor/PVR), melanoma cell adhesion molecule (MCAM), and desmoglein 2 (DSG2), which were higher in iMSC and UC.MSC secretomes; and secreted frizzled-related proteins 4 (SFRP4) and cystatin 2 (CST2) which were strongest in BM.MSC and AT.MSC secretomes **(Fig. S7a-e)**. The other principal component of variability (PC2, 17.45% of variation) showed separation of UC.MSC and AT.MSC secretomes from the iMSC and BM.MSCs and was driven by increased CXCL1 and retinoic acid receptor responder 1 (RARRES1), and reduced COL5A3, Wnt family member 5A (WNT5A) and growth differentiation factor (GDF6) in UC.MSC and AT.MSC secretomes **(Fig. S8a-e)**.

To further identify patterns in the expression level of proteins secreted by MSCs from different sources, two-way heat maps were generated, and K-means clustering was used to group proteins with similar expression patterns, forming six specific clusters **(**Fig. 4c**)**. Consistent with the PCA, the heatmap clustering showed the iMSC secretome to be distinct from that of tissue-derived MSCs. Of these, UC.MSCs bore the most similarity to the iMSCs, whilst the AT.MSC and BM.MSC were very different to the iMSCs but had profiles that were closely aligned to each other. To determine whether the proteins within the six clusters had shared biological functions, they were queried for enrichment of BP terms. Clusters one and five contained proteins that segregated iMSCs and UC.MSCs from AT.MSCs and BM.MSCs. The proteins in cluster one were higher in AT.MSC and BM.MSCs, and were overrepresented in fibrotic

processes including: '*extracellular matrix organisation*', '*regulation of proteolysis*', and '*tissue development*', whilst those in cluster five were lower in AT.MSC and BM.MSCs and were overrepresented in developmental processes such as '*heart morphogenesis*' and '*striated muscle tissue development*'. The proteins in clusters two and three were strongest in iMSC secretomes and were overrepresented in processes indicating stem cell-like properties and telomerase activity, including: '*regulation of protein localization to Cajal body*', '*positive regulation of establishment of protein localization to telomere*', and '*positive regulation of protein localization to chromosome telomeric region*'. In contrast proteins in cluster six, which were enriched in tissue-derived, but not iMSC, secretomes, were overrepresented in both pro-inflammatory and skeletal tissue developmental processes, including: '*complement activation*', '*humoral immune response*', '*cartilage development*' (Fig. 4d) **(Tab. S3)**. The variation in functional enrichment between the secretomes of MSCs from different sources highlights the more stem-cell like and developmental identities of iPSC and UC.MSCs which contrasts with the more structural and homeostatic identities of adult tissue-derived MSCs, highlighting the need to carefully consider MSC source to effectively target desired outcomes.

The data was then interrogated to determine how MSC source affects the composition of the secretome after inflammatory licencing. Across the licensed secretomes, 418 proteins (60.8%) were conserved between all sources, which was very similar to the 59.2% conservation measured for the resting secretomes. Also bearing similarity to the resting MSCs, the licenced iMSCs secretomes had the most distinct secretome, containing 78 unique proteins, followed by UC.MSC secretomes with six unique proteins, AT.MSC secretomes with four unique proteins, and BM.MSC secretomes with just three unique proteins (Fig. 5a). The coefficient of variation (CoV) between licensed MSC lines also showed less variability between the batches of iMSC secretomes (CoV 17%) than observed for secretomes from different donors of BM.MSCs (CoV 40%), UC.MSCs (CoV 30%) or AT.MSCs (CoV 44%) **(Fig. S6b)**.

PCA of the licensed secretomes showed a similar pattern to the resting samples, with greater similarity between the iMSC and UC.MSCs, and separation of these from BM.MSC and AT.MSC secretomes along PC1 (55.36% of overall variation) (Fig. 5b). This separation of iMSC and UC.MSC secretomes from the adult-tissue derived secretomes was driven by reduced expression of PENK, CST2, complement factor D (CFD) and C-type lectin domain family 3 member B (CLEC3B), and increased levels of eukaryotic translation initiation factor 6 (EIF6), which was highest in the iMSC followed by UC.MSC secretomes **(Fig. S9a-e)**. The second principal component of variability (PC2, 13.18% of variation) separated the UC.MSC secretomes from all other cell sources and was driven by increased CXCL6 and decreased CXCL12, CX3CL1, and glucosamine (N-acetyl)-6-sulfatase (GNS). Interestingly, UC.MSC and BM.MSC secretomes, as well as commercial but not clinical-grade iMSCsecretomes shared concentrations of nucleotide exchange factor SIL1 (SIL1), a protein processing protein that has been previously identified at a transcriptomic level in certain suppopulations of MSCs[58] **(Fig. S10a-e)**.

Hierarchical clustering of the proteomic profiles supported the PCA findings in showing the greatest similarity between BM.MSC and AT.MSC secretomes and separation of these from the iMSC and UC.MSC secretomes. As was done for the resting secretome, proteins were grouped into six K-means clusters to

identify expression patterns and uncover distinct functional modules within the licensed secretome of MSCs from different sources (Fig. 5c). The biological functions of these K-means clusters were explored by GO enrichment analysis of BP terms. Cluster one consisted of 11 proteins which were highest in UC.MSC secretomes, likely responsible for the separation of UC.MSC secretomes from those of other MSC lines along PC2. While this represents a unique signature of the licensed UC.MSC secretome, the functions of these proteins did not converge on any particular process and no BP terms were significantly overrepresented by these proteins. Clusters two and four included proteins most strongly expressed in iMSC and UC.MSC secretomes, with the proteins in cluster two being more strongly upregulated than those in cluster four. The proteins in these clusters were likely responsible for the separation these from the AT.MSC and BM.MSC secretomes and were overrepresented in processes indicating stem/progenitor-cell like properties and telomerase activity, with those in cluster two including '*regulation of telomere maintenance via telomerase*', and '*telomere maintenance via telomerase*', while those in cluster four were overrepresented in *oxaloacetate metabolic process* and multiple processes pertaining to the '*regulation of protein localisation to telomere and Cajal body*'. Notably, the maintenance of telomere length is crucial for sustained cell division and the delay of senescence, it is a characteristic feature of highly proliferative stem cell populations and suggestive that the strong regenerative potential of both iMSC/UC.MSCs, but not BM.MSC/AT.MSCs, is maintained under both resting and licensed conditions[59]. Proteins in cluster five were weakly enriched in tissue-derived secretomes compared to iMSCs and were overrepresented in process linked to cell adhesion and ECM, including '*positive regulation of integrin mediated signalling*', '*extracellular matrix assembly*', and '*transforming growth factor beta 1 production*'. Finally, proteins in cluster three, which were upregulated in BM.MSC and AT.MSC secretomes, were overrepresented in '*defence response*', '*response to other organism*', and '*positive regulation of protein phosphorylation*' (Fig. 5d) **(Tab. S4)**. This suggests that, despite the largely conserved secretory profile of licensed MSC secretomes, there are still differences in expression of specific factors between MSCs from different sources. Overall, however functional enrichment indicates that across licensed MSCs secretomes, most of the source-based variation continues to be driven by the activity of telomerase in iMSC, and to a lesser extent UC.MSCs, and the secretion of matrix proteins by AT.MSC and BM.MSCs.

Comparison of functional immunomodulatory and proregenerative capacity of MSC CM

Due to the differences in the proteins expressed by resting and licenced MSCs, and the clear involvement of these in pro-regenerative and immunomodulatory processes, the effects of the resting and licensed CM were assessed using functional assays of pro-regenerative and immunomodulatory capacity.

The ability of MSCs to inhibit T-cell proliferation is a key aspect of their immunomodulatory identity[50] and activated pan T-cells were treated with resting or licensed CM from the different MSC sources. Regardless of source, the resting CM did not significantly inhibit T-cell proliferation, indicating that without adequate inflammatory licensing MSCs do not produce the necessary factors to perform this function. In contrast, the licensed CM significantly inhibited T-cell proliferation regardless of MSC source. However, the iMSC CM more effectively reduced T-cell proliferation in comparison to tissue-derived MSC CM, with an 11.7% reduction from BM.MSC CM, 8.1% from UC.MSC CM, and 5.5% from AT.MSC CM (Fig. 6a). Overall, the

ability to inhibit T-cell proliferation correlated strongly with the acquisition of an MSC2 phenotype. This mirrored the amount of IDO produced, which was only detected at significant levels under licensed conditions, and which was similarly higher in iMSC secretomes compared to BM.MSC secretomes.

In contrast, the pro-regenerative potential of the MSC secretome was exemplified by their ability to promote proliferation and migration of fibroblasts in a scratch wound assay (Fig. 6b). While resting MSC CM from all sources significantly reduced cumulative wound size compared to fresh media this was not observed in cultures treated with licensed CM. Licensed BM.MSC CM actually lessened the wound closure as compared unconditioned controls. Under resting conditions, both iMSC and UC.MSC CM ($p = < 0.001$) were more beneficial for wound closure than either BM.MSC or AT.MSC CM (Fig. 6c). Correspondingly, the pro-regenerative potential of the MSC secretome was negatively correlated to the acquisition of an MSC2 phenotype. This suggests that the proteins downregulated during the MSC2 licensing process, including collagens and other ECM proteins, may be key in the pro-regenerative potential of the MSC secretome. Together, these results support the hypothesis that MSCs exhibit a strong phenotypic switch upon inflammatory licensing, from a pro-regenerative to immunomodulatory phenotype, and that the key benefits of these two secretomes may be mutually exclusive.

3 Discussion

This study used high resolution two-dimensional LC-MS/MS to profile MSC secretomes from multiple sources under both resting and inflammatory licensed conditions. The data generated describes a conserved profile of MSC2 inflammatory licensing and presents a detailed atlas of MSC secretomes across multiple tissue sources, donors, and iPSC-platforms. Importantly, this study shows for the first time that immunomodulatory plasticity and the MSC2 phenotype are recapitulated by iPSC-derived MSCs. This fills a critical gap in our understanding of MSC biology and yields new insights into the defining criteria of these cells. Furthermore, this dataset serves as a robust framework to compare and predict the therapeutic potential of different MSCs, allowing the identification of optimal candidates from specific target applications.

The panel of MSC lines used in this study enabled the first comparison of the secretome of iMSCs to those derived from tissues. The inclusion of independent batches of clinical-grade iMSCs and a commercially available iMSC line also permitted investigation into the potential differences between batches of iMSCs, something that was previously unknown. Moreover, the selection of bone marrow, adipose, and umbilical cord-derived MSCs covered the most common sources of MSCs and provided insights into differences between MSCs derived from adult and natal tissues (i.e. varying *in vivo* age). Finally, by including MSCs from multiple donors/batches, our dataset enabled conclusions to be made regarding the consistency of the secretome in relation to donor or batch variability. All MSCs were cultured in parallel to passage six to allow sufficient expansion of tissue-derived MSCs and align them with clinical iMSC batches, which are administered after passage five. At this point, all MSC lines were confirmed to have maintained a fibroblastic morphology and proliferative capacity, indicating that they had not reached senescence. They also adhered to the ISCT minimal criteria, expressing appropriate

surface antigen profiles, and demonstrating *in vitro* tri-lineage differentiation. Importantly, while all the MSC lines included in this study met the ISCT minimal criteria[3], there were still stark differences in their secretory profiles and immunomodulatory potential which reinforces the need to understand the differences between MSC sources and the potential therapeutic impact this may have.

iMSCs and tissue-derived MSCs undergo inflammatory licencing

While MSC plasticity is central to both their *in vivo* identity and therapeutic potential, only a limited number of studies have previously addressed this, leaving much to be understood about the process of MSC licensing and the differences between the different MSC subtypes. In this study, all MSC lines, including both clinical and commercially available iMSCs, licensed to an MSC2 immunosuppressive phenotype after 48 h exposure to 15ng/mL IFNγ and 15ng/mL TNFα. Following the accepted markers for MSC licencing, this was verified by upregulation of HLA-DR and HLA-ABC surface markers and the increased secretion of IDO[10,12,14,]. These indicators are well characterised across tissue-derived MSCs[34,36,62–66] but have not previously been demonstrated in iMSCs. The demonstration of phenotypic plasticity by iPSC-derived MSC populations is hugely important for their successful application as a cell therapy as this process underpins the immunomodulatory properties of MSCs and the mechanisms by which they are thought to act in many of their target applications[67]. This comparable response to inflammatory factors also validates the equivalency of iMSCs to tissue-derived MSCs in one of the most fundamental and complex MSC behaviours, and further supports the potential for iMSCs to be applied in many of the contexts where tissue-derived MSCs have shown promise. Considering the MSC panel as a whole, the observed conservation of inflammatory licencing in MSCs isolated from such a diverse range of sources emphasizes their overlapping biological roles and contributes to the deeper understanding of fundamental MSC biology required to optimise their therapeutic potential.

A conserved signature of MSC2 inflammatory licencing

The paired resting and licensed MSC secretomes allowed a conserved proteomic signature of MSC2 licensing to be identified, highlighting 43 proteins as key markers of this process. When analysing the biological processes that these are involved with, there was a clear distinction between the resting and licenced secretomes where resting MSC secretomes reflected a developmental, regenerative and tissue homeostatic role, while licensed MSC secretomes reflected an immunomodulatory one. Broadly, this supports Waterman's model of MSC polarisation, where resting MSCs provide tissue repair and regenerative functions while the MSC2 phenotype regulates immunomodulatory processes and resolves inflammation[11–13,68]. Interestingly, the licensed MSC secretome contained both pro and anti-inflammatory factors, suggesting that chemotactic factors may function to attract peripheral immune cells while immunomodulatory factors such as IDO, IL18BP, and TSG6 simultaneously restrain the immune response. Inflammatory licencing also increased the concentration and complexity of the MSC secretome, with the licenced samples containing more individual proteins and at higher concentrations, likely reflecting the more complex and diverse signalling and behaviour of the MSC2 phenotype.

Despite the overall increase in complexity of the licensed MSC secretomes, there was a specific decrease in pro-regenerative proteins such collagens 1A1, 1A2, and 2A1, prostaglandin receptors, and thrombospondins. This was consistent with our functional testing in which licensed, but not the resting, secretomes inhibited T-cell proliferation *in vitro* while CM from resting MSCs more effectively induced proliferation and *in vitro* wound closure by fibroblasts, likely due to the increased secretion of ECM proteins. Though the concept that CM from resting MSCs is generally not immunomodulatory and will not inhibit T-cell proliferation is embedded in many publications[11,12,27,48,69–72], the need for inflammatory licensing of MSCs, either by cytokine stimulation, TLR agonism, or direct contact with activated immune cells, is often not explicitly described, leading to a continued lack of clarity surrounding best practices and the different roles and functions of MSC secretomes. By identifying enriched TF binding motifs, it was also possible to provide insights into the regulatory mechanisms involved in MSC phenotypic plasticity. The key TF networks in resting MSCs (SP3, KLF13, and SOX4) are commonly associated with the regulation of cell proliferation, differentiation, and maintenance of cell identity[73–75]. They may also play a role in the differentiation potential of resting MSCs, which has been reported to decrease with inflammatory licensing[76]. In contrast, the key TFs connected to the licenced secretome (IRF, Rel, and NF-κB family) are known regulators of immune responses and inflammatory signalling. Specifically, IRF and NF-κB signalling drive the inflammatory response that results from TLR stimulation[53,77], while REL, RELA, and RELB form complexes with NF-κB, modulating the specificity and intensity of the resulting inflammatory response[78]. The activity of these regulatory networks implies that the switch to an MSC2 phenotype is driven by NF-κB signalling pathways, which can be activated by either inflammatory cytokines or TLR3/4 activation.

The MSC secretome varies with MSC source

Importantly, our findings showed that the source of MSCs was responsible for more of the variability in the MSC secretome than the functional phenotype. This is of considerable interest considering the substantial differences between resting and licensed MSCs and underscores the critical importance of comprehending variability of MSC source, especially in the context of developing MSC therapies. Previously, it has not been possible to make this comparison as no prior studies have characterised the secretome of both MSC source and inflammatory phenotype in parallel. The separation of adult and natal tissue-derived MSC secretomes aligns with observations by Shin et al. who also reported that the secretome of natal tissue-derived MSCs (placenta derived and Wharton's jelly derived-MSCs) is more diverse than that of adult tissue-derived MSCs (BM.MSCs and AT.MSCs)[45]. Kehl et al. also specifically linked the complexity of CM from Wharton's jelly-derived MSCs to a more complete angiogenic network and higher concentrations of angiogenesis-related proteins than were identified in either BM.MSC or AT.MSC derived CM[79]. Corresponding with our findings, these suggest that some MSC lines may be more potent due simply to a greater proteomic output.

Under resting conditions, a key difference between the secretomes of iMSC/UC.MSCs and those of the adult-tissue derived MSCs was driven by secretion of proteins involved in telomerase activity and

DNA/RNA metabolic processes. Enrichment of these processes emphasizes the highly proliferative, and translationally active nature of the iMSCs and UC.MSCs, correlating with an observed increase in protein secretion. This may be related to *in vivo* MSC age, representing a more stem-like phenotype associated with 'younger' MSCs. Supporting this is the finding that MCAM and DSG2, which were highest in iMSC/UC.MSC secretomes, have been linked to maintenance of a stem-like phenotype[80], while PENK, which was highest in BM.MSC/AT.MSC secretomes, has been linked to senescent or aged MSCs[81–83]. Confirming that these changes have functional effects, CM from the iMSCs and UC.MSCs, which displayed a "younger" profile, increased the proliferation of human dermal fibroblasts to a greater extent than those derived from adult tissue sources. BM.MSC/AT.MSC secretomes were characterised by the upregulation of proteins linked to ECM structure and organisation and proteolytic processes, suggesting active involvement in tissue repair and microenvironment maintenance. This may explain the increased proliferation and migration of fibroblasts in response to these secretomes and suggest their advantage for tissue-forming applications, although increased secretion of ECM proteins may also contribute to fibrotic signalling pathways.

Telomerase activity and DNA/RNA biosynthetic processes remained a key difference between iMSC/UC.MSC and adult tissue-derived secretomes after inflammatory licencing. Despite the broad upregulation of immunomodulatory proteins in licensed secretomes, some differences in the levels of specific immunomodulatory proteins were observed. Licensed UC.MSC secretomes contained different concentrations of several chemotactic factors, suggesting that they may be comparatively more chemotactic towards neutrophils than other MSCs, but less chemotactic towards lymphocytes and monocytes. While the chemotactic effect of UC.MSCs has not been directly compared with that of MSCs from other sources, general differences in the mechanisms by which they exert their immunomodulatory effects has been described. Song et al. reported an increase in IL6 and prostaglandin E2, in UC.MSC secretomes in comparison to BM.MSC secretomes. Despite this they also reported that UC.MSCs were able to functionally exert comparable immunomodulatory effects[84]. Overall, the variations in MSC secretory profiles mirror distinct physiologies of the MSC source, with iMSCs and UC.MSCs producing a secretome that reflects natal tissue origins and the effective regression of *in vivo* age that occurs with iPSC-based technologies[85,86], while older, adult tissue-derived MSC secretomes reflect tissue homeostatic and fibrotic phenotypes.

Different MSC secretomes have distinct functional effects

Ultimately, the differences in MSC secretome are important due to the functional effects that they exert. Importantly, our data confirmed that there were differences in target cell response, when treated with the resting and licensed CM, or CM from different MSC sources. For example, only the licensed CM could reduce T-cell proliferation while the resting CM better promoted wound closure. This supports that premise that the immunomodulatory properties of the MSC secretome are present only after inflammatory licensing and that the resting secretome more effectively promotes pro-regenerative and wound healing processes[11,12,50,60]. Similar functional differences between MSC sources have been

identified before, for example in a comparison of BM.MSCs, AT.MSCS, Wharton's jelly and placenta-derived MSCs, where BM.MSCs provoked the least potent suppressing T-cell proliferation [87]. However, it has so far not been possible to link these with the composition of the secretome, a step which provides new insights into the biological mechanisms that underpin these differences. Using our rich dataset, differences in the functional capacity of different MSC sources and states could also be correlated with the proteomic profiles. For example, the iMSC and UC.MSC CM resulted in faster wound closure than AT.MSC or BM.MSC CM under both resting and licensed conditions and these functional differences correlated with the increased protein complexity of their secretomes and the enrichment of proteins known to promote proliferation and migration (MCAM, DSG2)[88,89]. This provides insights into the likely molecular mechanisms governing this process. Such information has substantial promise to inform the development of more effective MSC therapies by identifying the source of MSCs most likely to secrete the proteins required, or even to define new molecular targets for pharmaceutical intervention.

4 Conclusion

This study presented a detailed atlas of resting and MSC2-licensed MSC secretomes across multiple tissue sources, donors, and iPSC-platforms. Importantly, we demonstrate for the first time that immunomodulatory plasticity and the MSC2 phenotype are recapitulated by iMSCs which supports their equivalency to tissue-derived MSCs in a process which is critical for their therapeutic potential. The data also identify a conserved profile of MSC2 inflammatory licensing in which resting MSCs produce a pro-regenerative secretome which rapids switches to an immunomodulatory profile upon inflammatory stimulation. In tandem, we describe the variations between MSC secretory profiles from different sources, where iMSC secretomes were most similar to UC.MSC secretomes, and AT.MSC and BM.MSC secretomes were most similar to each other. This reflects distinct physiologies of MSC sources, with strong emphasis on *in vivo* age and provides valuable fundamental insights into MSC heterogeneity. Collectively, this comprehensive data on the composition of MSC secretome provides insights into the molecular mechanisms underlying the therapeutic effects of MSCs and the differences by source and functional state. This can be used to inform the design of more effective MSC-based therapies by identifying the most suitable MSC source for a particular application, allowing the development of tailored culture conditions and/or preconditioning methods to enhance the therapeutic potential of these cells, or even identifying specific factors that can be adapted for pharmaceutical intervention.

5 Materials and methods

Derivation of the MSC working panel

A working panel of MSC populations was created, with 13 human MSC populations, including three donors of bone marrow, adipose tissue and umbilical cord,-derived MSCs, three independent batches of Cynata Therapeutics' clinical iMSC product, CYP001, and one batch of commercial-grade iMSCs, purchased from Cellular Dynamics Incorporated (CDI).

Bone marrow-derived MSCs

Three donors of bone marrow-derived MSCs, donor IDs 18TL113327 (BM.MSC 1), 0000684888 (BM.MSC 2), and 0000539540 (BM.MSC 3), were purchased at P2 (Lonza; #PT-2501). P2 vials were thawed as per manufacturer's instructions and plated in a T175 flask in MSC basal medium consisting of DMEM with 10% fetal bovine serum (FBS).

Adipose tissue-derived MSCs

Human adipose tissue samples were taken from the lower abdomen of patients undergoing routine C-section with informed consent (Ritchie Centre Human TissueBank, Hudson Institute of Medical Research, HREC reference 12387B). Tissue was kept at RT and processed within four h of collection. Briefly, the tissue was washed using DPBS (ThermoFisher; #14040216) supplemented with 1x Antibiotic-Antimycotic containing 100 units/mL of penicillin, 100 µg/mL of streptomycin, and 0.25 µg/mL of Gibco Amphotericin B (AA) (ThermoFisher; #15240062), mechanically dissociated using scalpel blades and collected in a 50 mL falcon tube. Dissociated tissue was digested in 2 mg/mL collagenase type I (Life Technologies; #A1064401) in DMEM) at 37°C for 1 h under gentle agitation. Digested samples were diluted 1:1 with MSC high glucose basal medium, sequentially filtered through 100 µm and 40 µm filters, and centrifuged to pellet the cells. This pellet was treated with 1:3 mixture of DMEM: erythrocyte lysis buffer (155 mM NH4Cl (ThermoFisher; #254134), 10 mM KHCO3 (Fisher Scientific; #P235-500), 0.1 mM ethylenediaminetetraacetic acid (EDTA) (ThermoFisher; #15575020) for 5 min. at RT. The remaining cells were resuspended in DMEM-HG (Gibco; #11965092) with 1% AA and 20% FBS ((Scientifix; #SFBS-AU) and plated at 2.5 x 10^3 cells/cm^2. Media was replaced after 24 h When SVF reached 70% confluence cells were detached using TrypLE (ThermoFisher; #12605010) for 3 min. at 37°C and replated at 2.5 x 10^3 cells/cm^2 at P0 in MSC basal media.

Umbilical cord-derived MSCs

Human umbilical cord tissue samples were collected with informed consent (Ritchie Centre Human TissueBank, Hudson Institute of Medical Research, HREC reference 12387B). Tissue was kept at RT and processed within four h. of collection. Briefly, the tissue was washed using DPBS (ThermoFisher; #14040216) supplemented with 1x AA (ThermoFisher; #15240062). Umbilical vein and arteries were removed using scalpel blades and the remaining Wharton's jelly and cord tissue was sectioned into 5 mm^2 explants. Explants were plated 1 per 5 cm^2 in a cell culture dish in DMEM-HG (Gibco; #11965092) with 1% AA and 20% FBS ((Scientifix; #SFBS-AU). Media was replaced after 24 h When outgrowth was visible (7–10 days) explants were removed and adhered cells were detached using TrypLE (ThermoFisher; #12605010) for 3 min. at 37°C and replated at 2.5 x 10^3 cells/ cm^2 at P0 in MSC basal media.

iPSC-derived MSCs

Three batches (CYN002, CYN004, and CYN005) of Cynata therapeutics' clinical-grade iMSC product CYP001™ were provided by Cynata Therapeutics'. P2 vials were thawed as per provider's

recommendations and plated in a T175 flask in MSC basal medium.

An additional batch of commercial-grade iMSCs (iCell Mesenchymal Stem Cells™) were purchased from Cellular Dynamics Incorporated USA (Cellular Dynamics; #R1098). P2 vials were thawed as per the manufacturer's recommendations and plated in a T175 flask in MSC basal medium.

MSC maintenance

MSC lines were cultured in MSC basal media at 37°C and 5% CO_2. All cultures were tested and confirmed free of mycoplasma every three months using a Mycoalert kit (LT07-118; Lonza). When cultures reached 80% confluence cells were detached using TrypleE Express Enzyme (ThermoFisher; #12604013) and passaged at a 1:4 ratio. All experiments were performed using passage six MSC lines and prior to all experiments, cells were serum-starved for 12 h in DMEM containing 0.5% FBS.

MSC characterisation and licensing

Multilineage differentiation of MSC lines was assessed by differentiation into osteocytes, adipocytes and chondroblasts as previously described[90][c]. After 21 days differentiated cell cultures were fixed and stained using i) Alizarin Red (Sigma Aldrich; #A5533), ii) Oil Red O (Sigma Aldrich: #O0625), or iii) Alcian blue (Sigma Aldrich; #A5268).

MSCs were characterize on surface markers recommended but the ISCT minimal criteria[3] CD14, CD19, CD34, CD45, CD73, CD90, CD105 and HLA-DR by flow cytometry. 5 x 10^5 MSCs were co-stained for 1 h at room temperature according to standard procedures with antibodies listed below. Thirty thousand events were acquired using LSR Fortessa X20 (BD Bioscience, USA) and data sets were analysed using FlowJo software (Tree Star, Inc., UCA).

MSC lines were plated in complete MSC basal media and allowed to adhere overnight before licensing. Licencing was performed by culturing MSCs in DMEM-LG supplemented with 10% heat inactivated FBS (HI-FBS, 58°C for 30 min) 15 ng/ mL hIFN-γ (Peprotech; #300-02) and 15 ng/mL hTNF-α (Peprotech; #300-01A) for 48 h. Resting MSCs were cultured in parallel in DMEM-LG supplemented with 10% heat inactivated FBS MSC.

Licensed phenotype was confirmed by flow cytometry analysis and quantification of IDO in conditioned media. After 48 h culture with or without hIFN-γ/ hTNF-α exposure, 3 x 10^5 MSCs were co-stained for HLA-DR and HLA-ABC for 1 h at room temperature according to standard procedures. Antibodies and concentrations are listed below. Thirty thousand events were acquired using LSR Fortessa X20 (BD Bioscience, USA) and data sets were analysed using FlowJo software (Tree Star, Inc., UCA).

Concentration of secreted IDO was assessed using human Indoleamine 2,3-dioxygenase IDO DuoSet enzyme-linked immunosorbent assay (ELISA) (RD systems; #DY6030B-05), as per the manufacturer's instructions.

MSC CM production and harvest

MSC lines were plated in complete MSC basal media and allowed to adhere overnight before MSC licensing. After 48 h the medium was aspirated and cells were washed gently three times in excess PBS. Conditioning medium (1 mL/ 1 x 10^5 cells), consisting of DMEM-LG, no phenol red (Gibco; #31053028) supplemented with 1:100 ITS (Sigma-Aldrich; # I3146-5ML) was added for a further 48 h before the conditioned media (CM) was collected and filtered using a 0.2 µm filter to remove cell debris. CM was processed for LC-MS/MS immediately or aliquots stored at -80°C for further analyses.

QC and proteomic profiling of MSC secretomes

Liquid chromatography tandem mass spectroscopy (LC-MSC/MS) experiments were performed by Monash Proteomics and Metabolomic Facility. Proteins were retrieved from 50 µl of CM using 5 µl Strata Clean resin beads per mL of CM (Agilent Technologies, USA) and further processed for in-gel digestion. 5µl peptide extract was analysed by LC-MS/MS on an EASY-nLC1000 chromatograph connected to a QExactive HF mass spectrometer (ThermoFisher Scientific) using a Pepmap100 Trap C18 300mm×5mm (Thermo Fisher Scientific) and a C18 separation column (3 µm, 100˚A, 75µm×15cm, Nikkyo Technos, Tokyo, Japan) by applying a 120 min. gradient.

LC-MS/MS data was processed with MaxQuant (version 1.5.4.1) using default settings for peak detection, strict trypsin cleavage rule allowing for up to three missed cleavages, variable oxidation on methionine, deamidation of asparagine and glutamine, and acetylation of protein N-termini with strict carbamidomethylation of cysteines. Match between runs was used within each sample group with a retention time window of 1 min. Label free quantification (LFQ) was performed using classical normalisation with LFQ separated into parameter groups. The fragment spectra were interpreted with the SwissProt Homo sapiens database (version 2016 04) accepting only protein identifications with at least two razor peptides at a 1% false discovery rate (FDR) cutoff.

Processing, analysis and visualisation of LC-MS/MS data

For LC-MS/MS data analysis, protein lists retrieved from MaxQuant pipeline were processed using LFQ Analyst[91], removing contaminant proteins, reverse sequences, proteins identified “only by site”, and those detected in the unconditioned media control (DMEM-LG + 1:100 ITS). Remaining protein lists were mapped to Gene Ontology term: extracellular space (GO:0005615) (GSEA database https://www.gsea-msigdb.org/gsea/msigdb/human/genesets.jsp?collection=GO:CC). to filter for secreted protein fractions. Where a protein was positively identified in two of three samples within a group the missing value was imputed as the median transformed intensity. Where proteins had at least one positive identification across all samples missing values were imputed from the low end of the Log2 transformed intensity distribution from each individual sample using Perseus (version 1.5.5.3) as suggested by Lazar et al.[92]. Data visualisation, differential expression and enrichment analysis were performed using iDEP 1.1[93] (http://bioinformatics.sdstate.edu/idep96/). K-means clustering was done using averge linkage, using the elbow methodology to determine optimal number of clusters. Limma package was used for identification

of differential expressed DE proteins between comparison pairs with an FDR cut off of 0.05 and a fold change ≥ 2.

Human fibroblast proliferation and migration assays

To assess the effect of resting and licensed CM on human fibroblast (HF) proliferation HFs were plated at 2 x 10^4 cell / cm^2 and allowed to adhere overnight. Media was exchanged for CM supplemented with 0.5% HI FBS and HF proliferation was assessed at days 1, 3, 5 and 7 using CellTiter 96® AQueous One Solution Cell Proliferation Assay (MTS) (Promega; #G3582) as per the manufacturer's instructions.

To assess the migration of HFs, an *in vitro* monolayer wound assay was conducted. HFs were seeded in 48-well plates in DMEM supplemented with 10% FBS until they reached confluence. Subsequently, a wound was made across the cultured cells using a 20 µl pipette tip. The culture medium was immediately replaced with CM. Cell migration was evaluated using time-lapse microscopy every 12 h. Wound closure was quantified by calculating the area under the curve (AUC) of wound closure over 72 h.

T-cell proliferation assays

To assess the ability of MSC CM to inhibit T-cell proliferation murine pan T-cells were isolated using Miltinye Pan T-cell Isolation Kits (Miltenyi Biotech; #130-095-130) as per the manufacturer's instructions. T-cells were plated at 2 x 10^4 cells per well in a 96-well U-bottom plate resuspended in DMEM-HG or CM with or without 5 ng/ mL Phytohaemagglutinin (PHA) (ThermoFisher; #00-4977-93). T-cells were cultured for 5 days at 37°C and 5% CO_2 before quantification of cell number using MTS reagent (Promega; #G3582) as per the manufacturer's instructions.

Declarations

Competing interests

The authors declare the following competing interests: K.K is an employee and shareholder of Cynata Therapeutics. The authors declare that this study received funding from Cynata Therapeutics. The funder was not involved in the study design, collection, analysis, interpretation of data, the writing of this article or the decision to submit it for publication, outside of the contributions of author K.K.

Author contributions

Conception and design of the study: M.H.G, J.E.F and K.K. Acquisition of data: M.H.G. Analysis and interpretation of data: M.H.G, J.E.F, M.J.M., M.M.M. and K.K. Initial draft and figure preparation: M.H.G. All authors were involved in drafting or revising the manuscript and have approved the final article.

Acknowledgments

M.H.G would like to thank Australian Government Research Training Program (RTP), Department of Materials Science and Engineering, Monash University and Monash Graduate Research Office, Monash University for financial support. This work was supported by the National Health and Medical Research Council (APP1140229 and APP1176213) to M.M.M, and the Viertel Charitable Foundation Senior Medical Researcher Fellowship to M.M.M. J.E.F. is a member of the ARC Training Centre for Cell and Tissue Engineering Technologies (IC190100026).The Australian Regenerative Medicine Institute is supported by grants from the State Government of Victoria and the Australian Government. The authors would also like to acknowledge support by facilities in the Monash Engineering Faculty and use of the Monash Proteomics and Metabolomics Facility and Monash Flow Core.

Data availability

Proteomics data generated for this study have been deposited in ProteomeXchange database. Source data are available with the paper and all other data or materials are available from the corresponding author upon reasonable request.

References

1. da Silva Meirelles, L., Chagastelles, P. C. & Nardi, N. B. Mesenchymal stem cells reside in virtually all post-natal organs and tissues. *J. Cell Sci.* **119**, 2204–2213 (2006).
2. McGrath, M. *et al.* GMP-compatible and xeno-free cultivation of mesenchymal progenitors derived from human-induced pluripotent stem cells. *Stem Cell Res. Ther.* **10**, 1–13 (2019).
3. Dominici, M. *et al.* Minimal criteria for defining multipotent mesenchymal stromal cells. The International Society for Cellular Therapy position statement. *Cytotherapy* **8**, 315–317 (2006).
4. Rehman, A. *et al.* Mesenchymal Stem Cells in Soft Tissue Regenerative Medicine: A Comprehensive Review. *Med. 2023, Vol. 59, Page 1449* **59**, 1449 (2023).
5. Merimi, M. *et al.* The Therapeutic Potential of Mesenchymal Stromal Cells for Regenerative Medicine: Current Knowledge and Future Understandings. *Front. Cell Dev. Biol.* **9**, 661532 (2021).
6. Wilson, A., Hodgson-Garms, M., Frith, J. E. & Genever, P. Multiplicity of Mesenchymal Stromal Cells: Finding the Right Route to Therapy. *Front. Immunol.* **10**, 1112 (2019).
7. Zhou, X., Jin, N., Wang, F. & Chen, B. Mesenchymal stem cells: a promising way in therapies of graft-versus-host disease. *Cancer Cell Int. 2020 201* **20**, 1–11 (2020).
8. Maxson, S., Lopez, E. A., Yoo, D., Danilkovitch-Miagkova, A. & LeRoux, M. A. Concise Review: Role of Mesenchymal Stem Cells in Wound Repair. *Stem Cells Transl. Med.* **1**, 142 (2012).
9. Sioud, M., Mobergslien, A., Boudabous, A. & Fløisand, Y. Mesenchymal stem cell-mediated T cell suppression occurs through secreted galectins. *Int. J. Oncol.* **38**, 385–390 (2011).
10. Krampera, M., Galipeau, J., Shi, Y., Tarte, K. & Sensebe, L. Immunological characterization of multipotent mesenchymal stromal cells—The International Society for Cellular Therapy (ISCT)

working proposal. *Cytotherapy* **15**, 1054–1061 (2013).

11. Krampera, M. Mesenchymal stromal cell licensing: A multistep process. *Leukemia* vol. 25 1408–1414 (2011).
12. Waterman, R. S., Tomchuck, S. L., Henkle, S. L. & Betancourt, A. M. A New Mesenchymal Stem Cell (MSC) Paradigm: Polarization into a Pro-Inflammatory MSC1 or an Immunosuppressive MSC2 Phenotype. *PLoS One* **5**, e10088 (2010).
13. Waterman, R. S., Henkle, S. L. & Betancourt, A. M. Mesenchymal stem cell 1 (MSC1)-based therapy attenuates tumor growth whereas MSC2-treatment promotes tumor growth and metastasis. *PLoS One* **7**, (2012).
14. Tomchuck, S. L. *et al.* Toll-Like Receptors on Human Mesenchymal Stem Cells Drive Their Migration and Immunomodulating Responses. *Stem Cells* **26**, 99–107 (2008).
15. Betancourt, A. M. & Waterman, R. S. The Role of Mesenchymal Stem Cells in the Tumor Microenvironment. *Tumor Microenviron. Myelomonocytic Cells* (2012) doi:10.5772/31933.
16. Noronha Nc, N. D. C. *et al.* Priming approaches to improve the efficacy of mesenchymal stromal cell-based therapies. *Stem Cell Res. Ther.* **10**, 1–21 (2019).
17. Mantovani, A., Sozzani, S., Locati, M., Allavena, P. & Sica, A. Macrophage polarization: Tumor-associated macrophages as a paradigm for polarized M2 mononuclear phagocytes. *Trends Immunol.* **23**, 549–555 (2002).
18. Martinez, C., Hofmann, T. J., Marino, R., Dominici, M. & Horwitz, E. M. Human bone marrow mesenchymal stromal cells express the neural ganglioside GD2: a novel surface marker for the identification of MSCs. *Blood* **109**, 4245–4248 (2007).
19. Mantovani, A. MSCs, Macrophages, and Cancer: A Dangerous Ménage-à-Trois. *Cell Stem Cell* **11**, 730–732 (2012).
20. Kopen, G. C., Prockop, D. J. & Phinney, D. G. Marrow stromal cells migrate throughout forebrain and cerebellum, and they differentiate into astrocytes after injection into neonatal mouse brains. *Proc. Natl. Acad. Sci. U. S. A.* **96**, 10711–10716 (1999).
21. Mackenzie, T. C. & Flake, A. W. Human mesenchymal stem cells persist, demonstrate site-specific multipotential differentiation, and are present in sites of wound healing and tissue regeneration after transplantation into fetal sheep. *Blood Cells. Mol. Dis.* **27**, 601–604 (2001).
22. Prockop, D. J. Repair of Tissues by Adult Stem/Progenitor Cells (MSCs): Controversies, Myths, and Changing Paradigms. *Mol. Ther.* **17**, 939–946 (2009).
23. Prockop, D. J., Kota, D. J., Bazhanov, N. & Reger, R. L. Evolving paradigms for repair of tissues by adult stem/progenitor cells (MSCs). *J. Cell. Mol. Med.* **14**, 2190–2199 (2010).
24. Iso, Y. *et al.* Multipotent human stromal cells improve cardiac function after myocardial infarction in mice without long-term engraftment. *Biochem. Biophys. Res. Commun.* **354**, 700–706 (2007).
25. Lee, R. H. *et al.* Intravenous hMSCs Improve Myocardial Infarction in Mice because Cells Embolized in Lung Are Activated to Secrete the Anti-inflammatory Protein TSG-6. *Cell Stem Cell* **5**, 54–63 (2009).

26. Gao, W.-X. *et al.* Effects of mesenchymal stem cells from human induced pluripotent stem cells on differentiation, maturation, and function of dendritic cells. *Stem Cell Res. Ther.* **8**, 48 (2017).
27. Fischer, U. M. *et al.* Pulmonary passage is a major obstacle for intravenous stem cell delivery: The pulmonary first-pass effect. *Stem Cells Dev.* **18**, 683–691 (2009).
28. Schrepfer, S., Deuse, T., … H. R.-T. & 2007, undefined. Stem cell transplantation: the lung barrier. *Elsevier*.
29. Lee, R. H., Oh, J. Y., Choi, H. & Bazhanov, N. Therapeutic factors secreted by mesenchymal stromal cells and tissue repair. *J. Cell. Biochem.* **112**, 3073–3078 (2011).
30. Eleuteri, S. & Fierabracci, A. Insights into the secretome of mesenchymal stem cells and its potential applications. *International Journal of Molecular Sciences* vol. 20 (2019).
31. Galderisi, U. & Giordano, A. The Gap Between the Physiological and Therapeutic Roles of Mesenchymal Stem Cells. *Med. Res. Rev.* **34**, 1100–1126 (2014).
32. Konala, V. B. R. *et al.* The current landscape of the mesenchymal stromal cell secretome: A new paradigm for cell-free regeneration. *Cytotherapy* **18**, 13–24 (2016).
33. Ranganath, S. H., Levy, O., Inamdar, M. S. & Karp, J. M. Harnessing the mesenchymal stem cell secretome for the treatment of cardiovascular disease. *Cell Stem Cell* **10**, 244–58 (2012).
34. Sandonà, M. *et al.* Mesenchymal Stromal Cells and Their Secretome: New Therapeutic Perspectives for Skeletal Muscle Regeneration. *Front. Bioeng. Biotechnol.* **9**, 319 (2021).
35. Vizoso, F. J., Eiro, N., Cid, S., Schneider, J. & Perez-Fernandez, R. Mesenchymal Stem Cell Secretome: Toward Cell-Free Therapeutic Strategies in Regenerative Medicine. *Int. J. Mol. Sci.* **18**, (2017).
36. Ahangar, P., Mills, S. J. & Cowin, A. J. Mesenchymal Stem Cell Secretome as an Emerging Cell-Free Alternative for Improving Wound Repair. *Int. J. Mol. Sci. 2020, Vol. 21, Page 7038* **21**, 7038 (2020).
37. Pinho, A. G., Cibrão, J. R., Silva, N. A., Monteiro, S. & Salgado, A. J. Cell Secretome: Basic Insights and Therapeutic Opportunities for CNS Disorders. *Pharm. 2020, Vol. 13, Page 31* **13**, 31 (2020).
38. Gnecchi, M., Ciuffreda, M. C., Malpasso, G., Musarò, P. & Turco, V. Mesenchymal Stem Cells. **1416**, (2016).
39. Gnecchi, M. *et al.* Evidence supporting paracrine hypothesis for Akt-modified mesenchymal stem cell-mediated cardiac protection and functional improvement. *FASEB J.* **20**, 661–669 (2006).
40. Aslam, M. *et al.* Bone Marrow Stromal Cells Attenuate Lung Injury in a Murine Model of Neonatal Chronic Lung Disease. *https://doi.org/10.1164/rccm.200902-0242OC* **180**, 1122–1130 (2012).
41. Goolaerts, A. *et al.* Conditioned media from mesenchymal stromal cells restore sodium transport and preserve epithelial permeability in an in vitro model of acute alveolar injury. *Am. J. Physiol. Lung Cell. Mol. Physiol.* **306**, (2014).
42. Rossi, D., Pianta, S., Magatti, M., Sedlmayr, P. & Parolini, O. Characterization of the Conditioned Medium from Amniotic Membrane Cells: Prostaglandins as Key Effectors of Its Immunomodulatory Activity. *PLoS One* **7**, e46956 (2012).

43. Han, Y. *et al.* The secretion profile of mesenchymal stem cells and potential applications in treating human diseases. *Signal Transduct. Target. Ther. 2022 71* **7**, 1–19 (2022).
44. Yen, B. L., Liu, K. J., Sytwu, H. K. & Yen, M. L. Clinical implications of differential functional capacity between tissue-specific human mesenchymal stromal/stem cells. *FEBS J.* (2022) doi:10.1111/FEBS.16438.
45. Shin, S. *et al.* Comparative Proteomic Analysis of the Mesenchymal Stem Cells Secretome from Adipose, Bone Marrow, Placenta and Wharton's Jelly. *Int. J. Mol. Sci.* **22**, 1–17 (2021).
46. Chan, J. L. *et al.* Antigen-presenting property of mesenchymal stem cells occurs during a narrow window at low levels of interferon-γ. *Blood* **107**, 4817–4824 (2006).
47. Sheng, H. *et al.* A critical role of IFNγ in priming MSC-mediated suppression of T cell proliferation through up-regulation of B7-H1. *nature.com*.
48. Krampera, M. *et al.* Role for Interferon-γ in the Immunomodulatory Activity of Human Bone Marrow Mesenchymal Stem Cells. *Stem Cells* **24**, 386–398 (2006).
49. Stagg, J., Pommey, S., Eliopoulos, N. & Galipeau, J. Interferon-γ-stimulated marrow stromal cells: a new type of nonhematopoietic antigen-presenting cell. *Blood* **107**, 2570–2577 (2006).
50. Galipeau, J. *et al.* International Society for Cellular Therapy perspective on immune functional assays for mesenchymal stromal cells as potency release criterion for advanced phase clinical trials. *Cytotherapy* **18**, 151–159 (2015).
51. Szklarczyk, D. *et al.* STRING v10: protein-protein interaction networks, integrated over the tree of life. *Nucleic Acids Res.* **43**, D447–D452 (2015).
52. Zhang, Q. *et al.* hTFtarget: A Comprehensive Database for Regulations of Human Transcription Factors and Their Targets. *Genomics. Proteomics Bioinformatics* **18**, 120 (2020).
53. Yanai, H., Negishi, H. & Taniguchi, T. The IRF family of transcription factors: Inception, impact and implications in oncogenesis. *Oncoimmunology* **1**, 1376 (2012).
54. de Jesús, T. J. & Ramakrishnan, P. NF-κB c-Rel Dictates the Inflammatory Threshold by Acting as a Transcriptional Repressor. *iScience* **23**, (2020).
55. Wang, G. *et al.* Kynurenic acid, an IDO metabolite, controls TSG-6-mediated immunosuppression of human mesenchymal stem cells. *Cell Death Differ.* **25**, 1209–1223 (2018).
56. Cao, Z., Sun, X., Icli, B., Wara, A. K. & Feinberg, M. W. Role of Krüppel-like factors in leukocyte development, function, and disease. *Blood* **116**, 4404 (2010).
57. Jones, K. *et al.* SOX4 and RELA Function as Transcriptional Partners to Regulate the Expression of TNF- Responsive Genes in Fibroblast-Like Synoviocytes. *Front. Immunol.* **13**, 789349 (2022).
58. Zhang, C. *et al.* Single-cell Transcriptomic Analysis Reveals the Cellular Heterogeneity of Mesenchymal Stem Cells. *Genomics. Proteomics Bioinformatics* **20**, 70 (2022).
59. Jing, S. *et al.* Application of telomere biology and telomerase in mesenchymal stem cells. *Nano TransMed* **1**, e9130007 (2022).

60. Krampera, M. *et al.* Immunological characterization of multipotent mesenchymal stromal cells-The International Society for Cellular Therapy (ISCT) working proposal. Manuscript ID CYTH-2012-0221 2 nd REVISION Immunological characterization of Multipotent Mesenchymal Stromal Ce. doi:10.1016/j.jcyt.2013.02.010ï.
61. Campioni, D. *et al.* A decreased positivity for CD90 on human mesenchymal stromal cells (MSCs) is associated with a loss of immunosuppressive activity by MSCs. *Cytom. Part B - Clin. Cytom.* **76**, 225–230 (2009).
62. Le Blanc, K., Tammik, C., Rosendahl, K., Zetterberg, E. & Ringdén, O. HLA expression and immunologic properties of differentiated and undifferentiated mesenchymal stem cells. *Exp. Haematol.* **31**, (2003).
63. Tse, W. T., Pendleton, J. D., Beyer, W. M., Egalka, M. C. & Guinan, E. C. Suppression of allogeneic T-cell proliferation by human marrow stromal cells: implications in transplantation. *Transplantation* **75**, 389–397 (2003).
64. Uccelli, A., Moretta, L. & Pistoia, V. Mesenchymal stem cells in health and disease. *Nat. Rev. Immunol. 2008 89* **8**, 726–736 (2008).
65. Nauta, A. J. & Fibbe, W. E. Immunomodulatory properties of mesenchymal stromal cells. *Blood* **110**, 3499–3506 (2007).
66. Klyushnenkova, E. *et al.* T cell responses to allogeneic human mesenchymal stem cells: immunogenicity, tolerance, and suppression. *Springer* **12**, 47–57 (2005).
67. Zhou, Y., Yamamoto, Y., Xiao, Z. & Ochiya, T. The Immunomodulatory Functions of Mesenchymal Stromal/Stem Cells Mediated via Paracrine Activity. *J. Clin. Med.* **8**, (2019).
68. Tomchuck, S. L. *et al.* Toll-like receptors on human mesenchymal stem cells drive their migration and immunomodulating responses. *academic.oup.com* **26**, 99–107 (2008).
69. Krampera, M. *et al.* Immunological characterization of multipotent mesenchymal stromal cells-The International Society for Cellular Therapy (ISCT) working proposal. Manuscript ID CYTH-2012-0221 2 nd REVISION Immunological characterization of Multipotent Mesenchymal Stromal Ce. *Cytoherapy* (2013) doi:10.1016/j.jcyt.2013.02.010ï.
70. Park, A. *et al.* Priming with Toll-like receptor 3 agonist or interferon-gamma enhances the therapeutic effects of human mesenchymal stem cells in a murine model of atopic dermatitis. *Stem Cell Res. Ther.* **10**, 1–11 (2019).
71. Rovira Gonzalez, Y. I., Lynch, P. J., Thompson, E. E., Stultz, B. G. & Hursh, D. A. In vitro cytokine licensing induces persistent permissive chromatin at the Indoleamine 2,3-dioxygenase promoter. *Cytotherapy* **18**, 1114–1128 (2016).
72. Kouroupis, D. *et al.* Infrapatellar fat pad-derived MSC response to inflammation and fibrosis induces an immunomodulatory phenotype involving CD10-mediated Substance P degradation. *Sci. Reports 2019 91* **9**, 1–16 (2019).
73. Tu, J. *et al.* UC-BSCs Exosomes Regulate Th17/Treg Balance in Patients with Systemic Lupus Erythematosus via miR-19b/KLF13. *Cells* **11**, (2022).

74. Zhang, L. *et al.* Sox4 enhances chondrogenic differentiation and proliferation of human synovium-derived stem cell via activation of long noncoding RNA DANCR. *J. Mol. Histol.* **46**, 467–473 (2015).
75. Aoyama, T. *et al.* Histone Modifiers, YY1 and p300, Regulate the Expression of Cartilage-specific Gene, Chondromodulin-I, in Mesenchymal Stem Cells. *J. Biol. Chem.* **285**, 29842 (2010).
76. Croitoru-Lamoury, J. *et al.* Interferon-γ Regulates the Proliferation and Differentiation of Mesenchymal Stem Cells via Activation of Indoleamine 2,3 Dioxygenase (IDO). *PLoS One* **6**, e14698 (2011).
77. Kawasaki, T. & Kawai, T. Toll-like receptor signaling pathways. *Front. Immunol.* **5**, 461 (2014).
78. Oeckinghaus, A. & Ghosh, S. The NF-κB Family of Transcription Factors and Its Regulation. *Cold Spring Harb. Perspect. Biol.* **1**, (2009).
79. Kehl, D. *et al.* Proteomic analysis of human mesenchymal stromal cell secretomes: a systematic comparison of the angiogenic potential. *Nat. Regen. Med.* **4**, (2019).
80. Jin, H. J. *et al.* Downregulation of Melanoma Cell Adhesion Molecule (MCAM/CD146) Accelerates Cellular Senescence in Human Umbilical Cord Blood-Derived Mesenchymal Stem Cells. *Stem Cells Transl. Med.* **5**, 427–439 (2016).
81. Bellayr, I. H., Marklein, R. A., Lo Surdo, J. L., Bauer, S. R. & Puri, R. K. Identification of Predictive Gene Markers for Multipotent Stromal Cell Proliferation. *Stem Cells Dev.* **25**, 861–873 (2016).
82. Bellayr, I. H. *et al.* Gene markers of cellular aging in human multipotent stromal cells in culture. *Stem Cell Res. Ther.* **5**, (2014).
83. Kulterer, B. *et al.* Gene expression profiling of human mesenchymal stem cells derived from bone marrow during expansion and osteoblast differentiation. *BMC Genomics* **8**, (2007).
84. Song, Y. *et al.* Human mesenchymal stem cells derived from umbilical cord and bone marrow exert immunomodulatory effects in different mechanisms. *World J. Stem Cells* **12**, 1032 (2020).
85. Conboy, I. M. *et al.* Rejuvenation of aged progenitor cells by exposure to a young systemic environment. *Nature* **433**, 760–764 (2005).
86. Simpson, D. J., Olova, N. N. & Chandra, T. Cellular reprogramming and epigenetic rejuvenation. *Clin. Epigenetics 2021 131* **13**, 1–10 (2021).
87. Li, X. *et al.* Comprehensive characterization of four different populations of human mesenchymal stem cells as regards their immune properties, proliferation and differentiation. *Int. J. Mol. Med.* **34**, 695–704 (2014).
88. Romanov, Y. A. *et al.* Comparative Analysis of Secretome of Human Umbilical Cord- and Bone Marrow-Derived Multipotent Mesenchymal Stromal Cells. *Bull. Exp. Biol. Med.* **166**, 535–540 (2019).
89. Hoang, D. H. *et al.* Differential Wound Healing Capacity of Mesenchymal Stem Cell-Derived Exosomes Originated From Bone Marrow, Adipose Tissue and Umbilical Cord Under Serum- and Xeno-Free Condition. *Front. Mol. Biosci.* **7**, (2020).
90. Vilar, A. *et al.* Substrate mechanical properties bias MSC paracrine activity and therapeutic potential. *Acta Biomater.* **168**, 144–158 (2023).

91. Shah, A. D., Goode, R. J. A., Huang, C., Powell, D. R. & Schittenhelm, R. B. Lfq-Analyst: An easy-To-use interactive web platform to analyze and visualize label-free proteomics data preprocessed with maxquant. *J. Proteome Res.* 204–211 (2019) doi:10.1021/ACS.JPROTEOME.9B00496/SUPPL_FILE/PR9B00496_SI_001.PDF.
92. Lazar, C., Gatto, L., Ferro, M., Bruley, C. & Burger, T. Accounting for the Multiple Natures of Missing Values in Label-Free Quantitative Proteomics Data Sets to Compare Imputation Strategies. *J. Proteome Res.* **15**, 1116–1125 (2016).
93. Ge, S. X., Son, E. W. & Yao, R. iDEP: an integrated web application for differential expression and pathway analysis of RNA-Seq data. *BMC Bioinforma. 2018 191* **19**, 1–24 (2018).

Figures

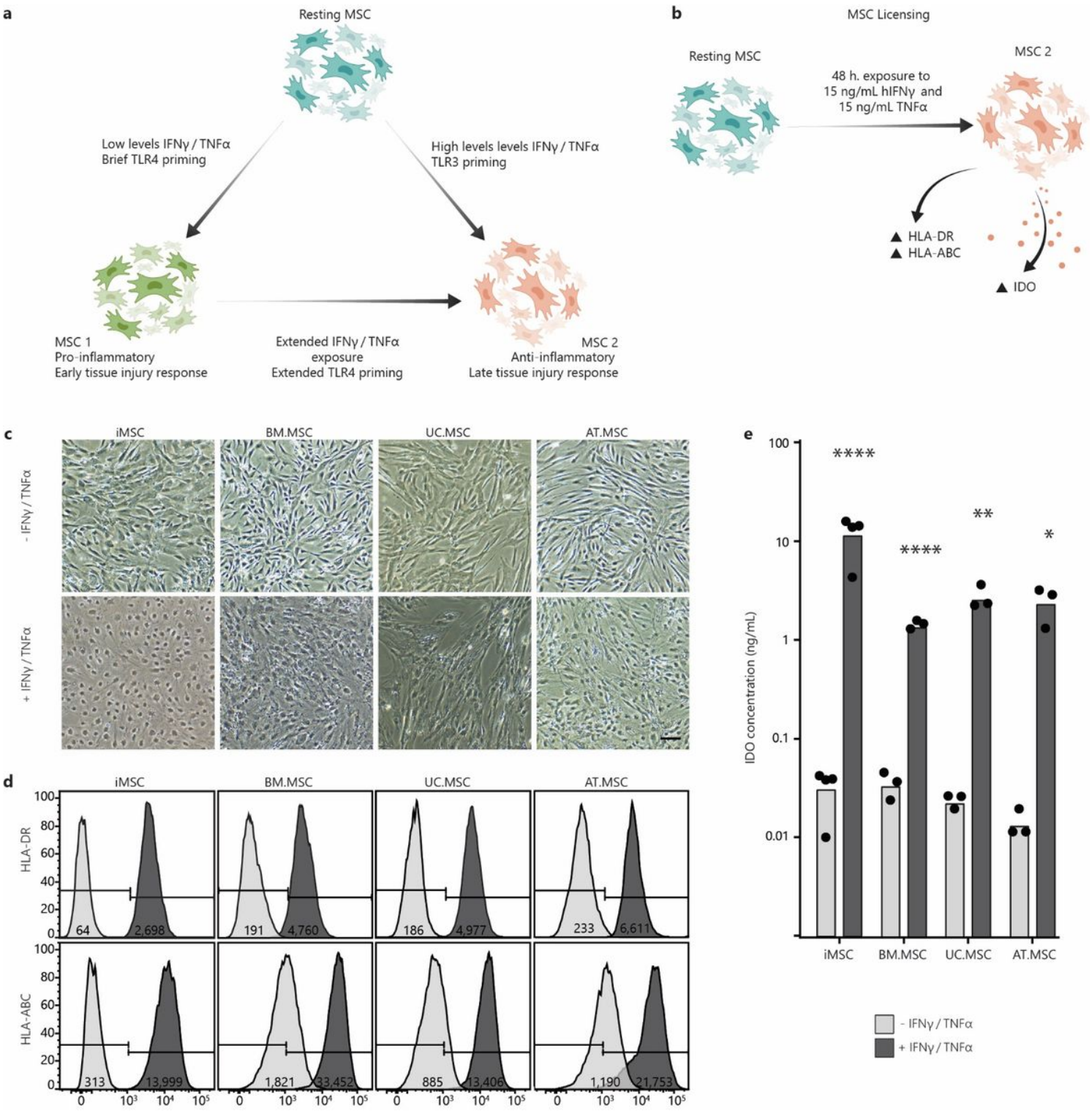

Figure 1

Inflammatory licensing of MSCs. (a) Schematic of the current model of MSC plasticity and MSC1/MSC2 licensing. **(b)** An MSC2 phenotype was achieved by exposing resting MSC lines to 15 ng/ml hIFNγ and 15 ng/ml hTNFα for 48 h and was characterised by increased expression of HLA-DR and HLA-ABC surface markers and secretion of IDO. **(c)** Bright field images of MSCs from different sources with and without exposure to inflammatory cytokines (scale bar, 25 μm). **(d)** Flow cytometry shift histograms of HLA-DR and HLA-ABC expression across MSCs from different sources with (+) (dark grey) and without (-) (light

grey) inflammatory cytokines. Histograms are representative of one MSC line per source, with data for replicate MSC lines presented in **Figure. S3**. **(e)** Bar chart shows concentration of IDO in CM with (+) (dark grey) and without (-) (light grey) inflammatory cytokines. Bars show the average concentration across MSC lines with individual points for the average (n=3 technical replicates) concentration for each MSC line. Statistical significance was calculated between each MSC line with and without exposure to cytokines by one-way ANOVA (*$p < 0.0332$, **$p < 0.0021$, ***$p < 0.0002$, ****$p < 0.0001$).

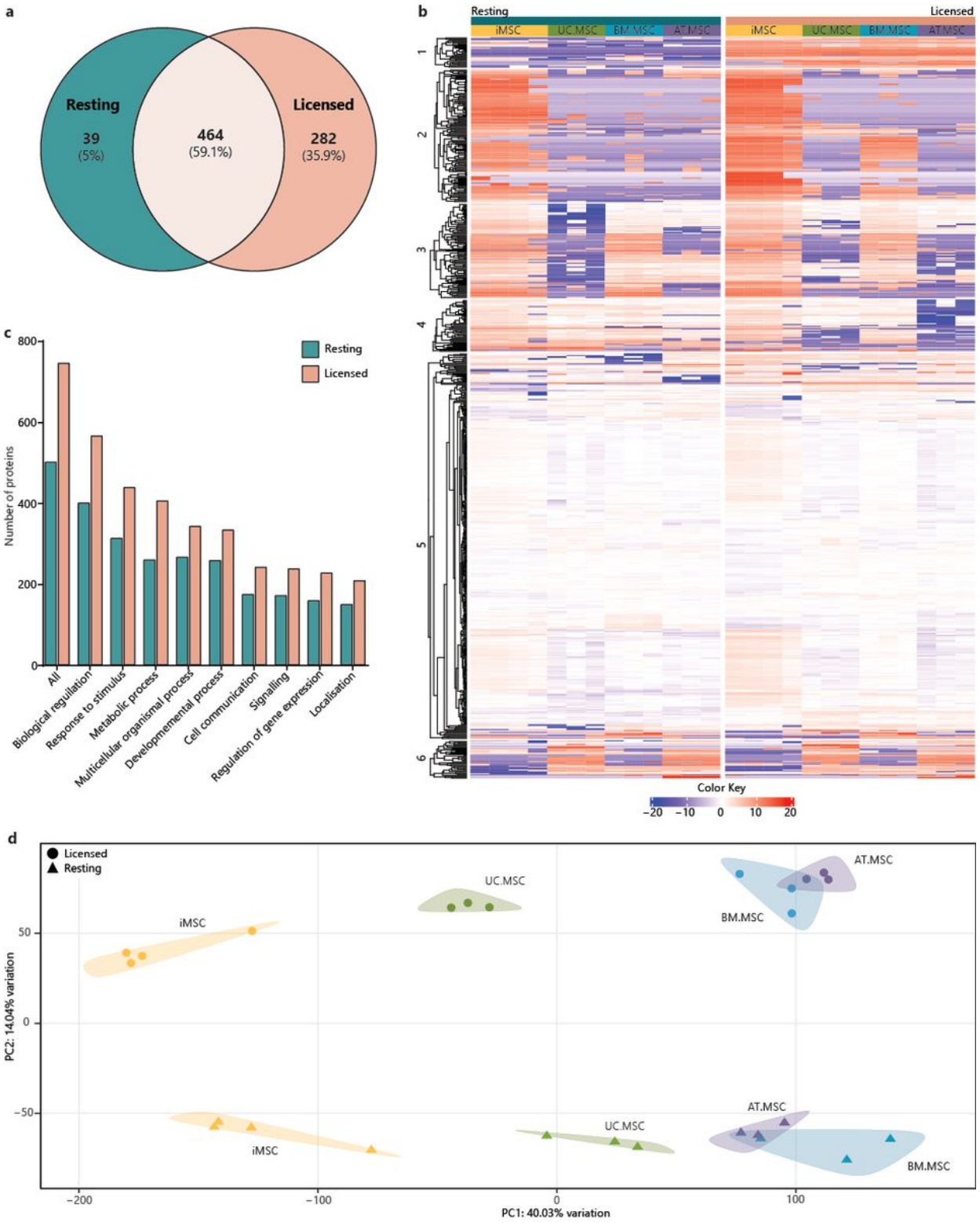

Figure 2

Characterisation of the MSC secretome by LC-MS/MS. (a) Venn diagram of the total number of secreted proteins in resting CM (teal) compared to licensed CM (coral). **(b)** Bar graph showing the numbers of proteins from resting (teal) and licensed (coral) CM annotated to the major GO biological process terms. **(c)** Heat map of proteomic profiles of MSC secretomes indicating protein intensity (red = more intense, blue = less intense). **(d)** PCA plot of relationships between MSC secretomes from different donors, sources and licensing phenotypes (iMSCs= yellow, UC.MSCs=green, AT.MSCs=purple, BM.MSCs=blue; Resting MSCs=▲, Licensed MSCs=●).

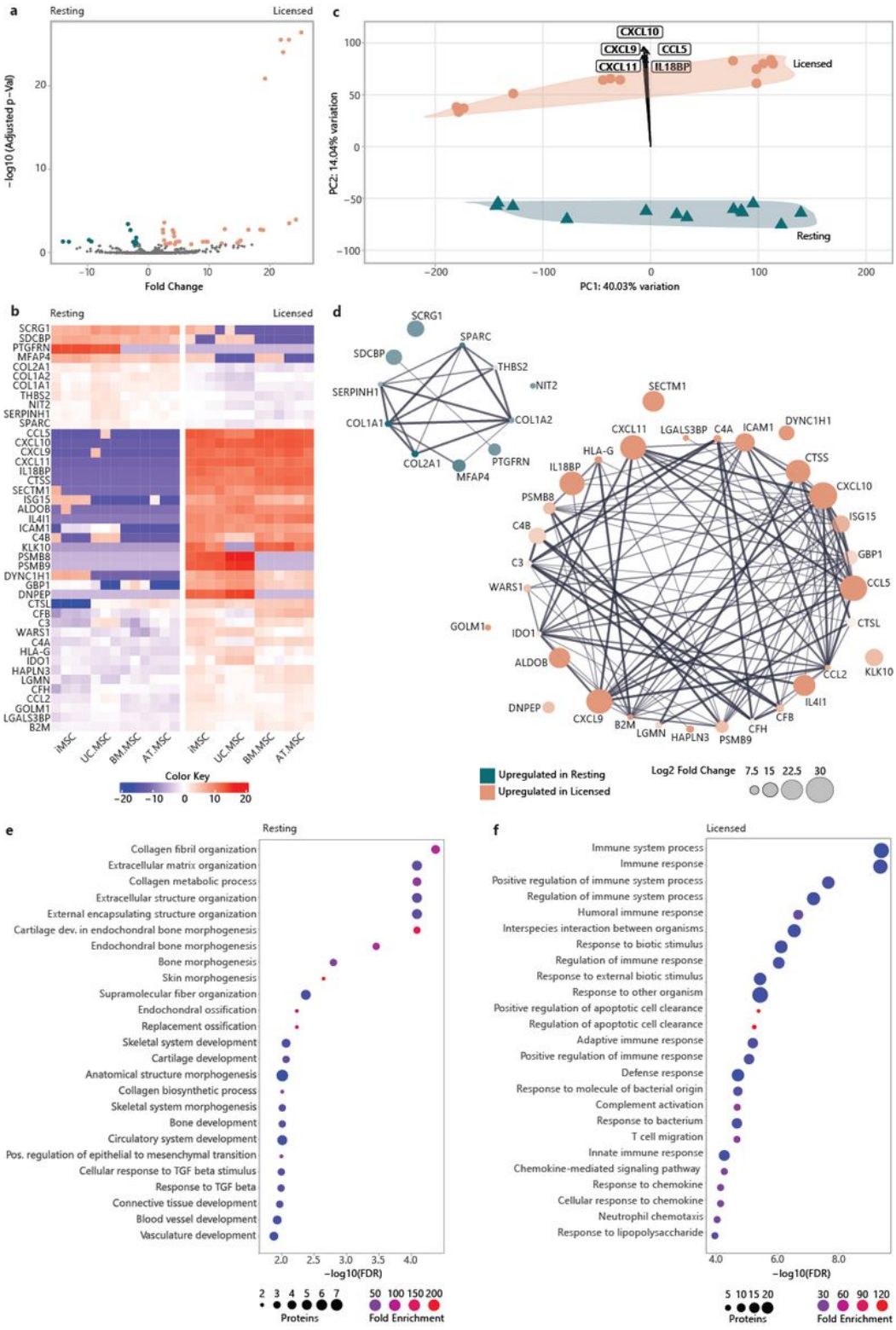

Figure 3

Comparison of resting and licensed MSC secretomes. (a) Volcano plot of fold change (x) versus statistical significance expressed as -log10(Adj.Pval) (y) of protein intensity between resting (teal) and licensed (coral) MSC secretomes. **(b)** Heatmap of protein intensity across MSC secretomes (x) (red = more intense, blue = less intense). **(c)** PCA loading plot showing specific proteins driving the separation of MSC sources along PC1 and resting (teal) vs licensed (coral) MSC secretomes along PC2. **(d)** Protein-

protein interaction plot illustrating the strength of interactions between proteins DE between resting and licensed secretomes. Node colour indicates whether proteins are upregulated in resting (teal) or licensed (coral) secretomes, node size indicates fold change, node transparency indicates significance (adjusted P value), edge thickness indicates interaction confidence. Bubble plots of overrepresented biological process terms in resting **(e)** and licensed **(f)** secretomes. The -log10 FDR is plotted on the x axis with fold enrichment indicated by bubble colour (red = greater enrichment, blue = less enrichment), and the number of annotated proteins indicated by the bubble size.

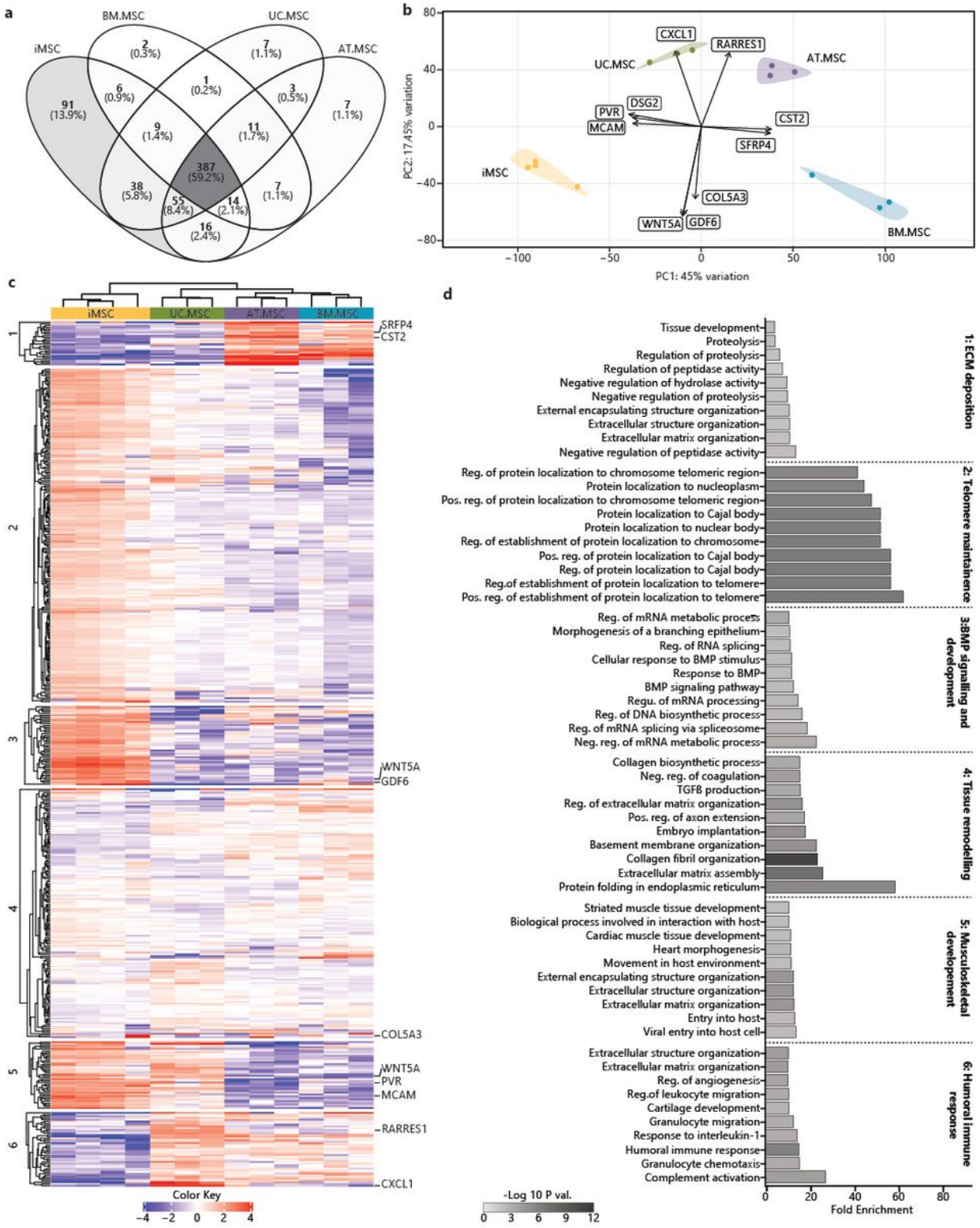

Figure 4

Heterogeneity of the resting MSC secretome between MSC sources. (a) Venn diagrams represent the total amount of identified proteins in CM from different sources (n=4 iMSC, n=3 BM.MSC, n=3 UC.MSC, n=3 UC.MSC), where more exclusive proteins were found in iMSC secretomes. **(b)** PCA loadings were plotted identifying specific proteins driving the separation of resting MSC secretomes by sources (iMSC=yellow, BM.MSC=blue, AT.MSC=purple, UC.MSC=green. **(c)** Heat map showing hierarchical Euclidean (average) clustering of resting MSC secretomes (x) and K-means clustering (n=6) of secreted proteins (y) based on intensity. Higher protein intensity is indicated in red and lower in blue. **(d)** Top 10 overrepresented GO BP terms for each K-means cluster of resting MSC secretomes were plotted as horizontal bar graphs. Bar length indicates fold enrichment, colour indicates significance (-log10 FDR) as per the legend.

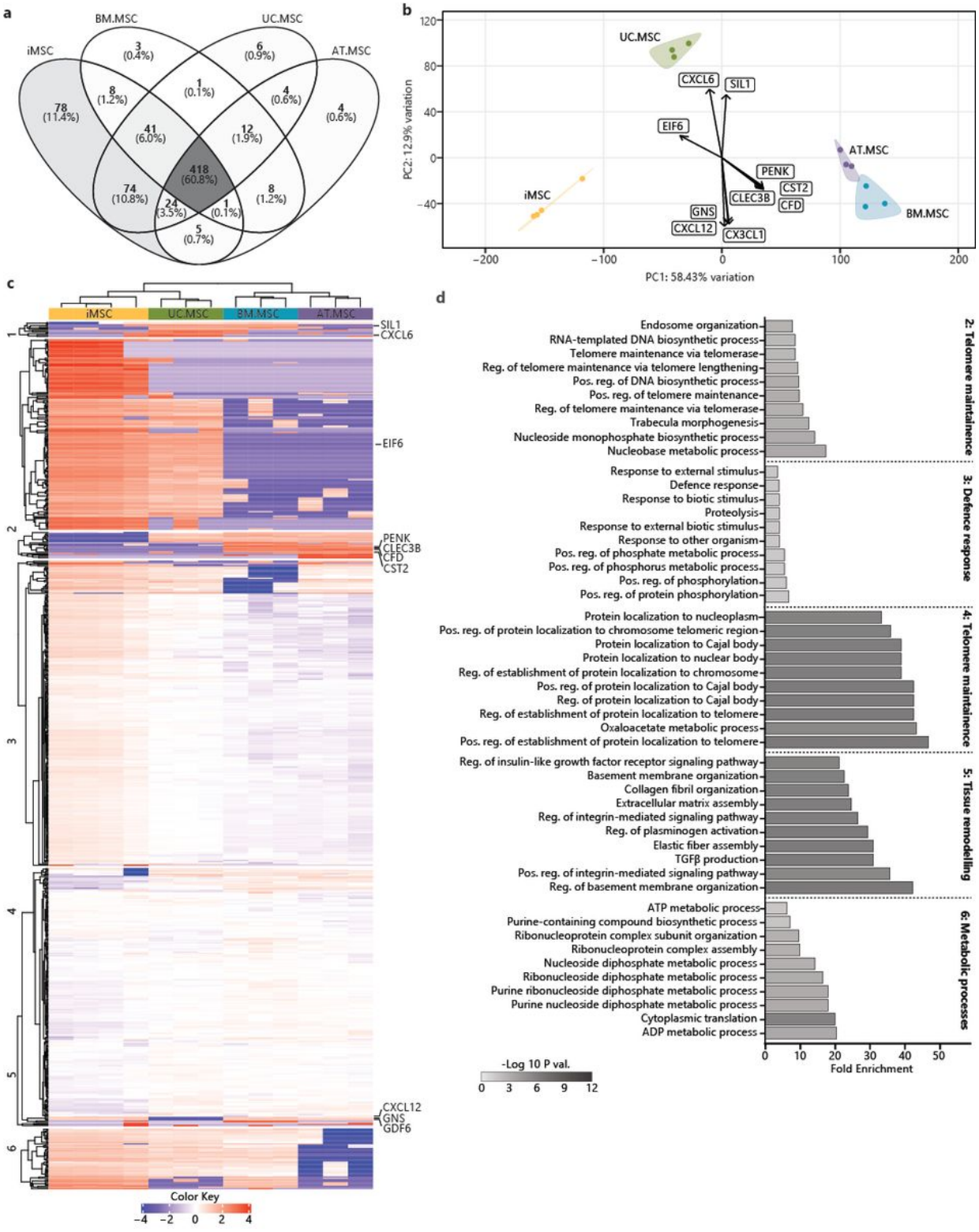

Figure 5

Heterogeneity of the licensed MSC secretome between MSC sources. (a) Venn diagrams represent the total amount of identified proteins in CM from different sources (n=4 iMSC, n=3 BM.MSC, n=3 UC.MSC, n=3 UC.MSC), where more exclusive proteins were found in iMSC secretomes. **(b)** PCA loadings were plotted identifying specific proteins driving the separation of licensed MSC secretomes by sources (iMSC=yellow, BM.MSC=blue, AT.MSC=purple, UC.MSC=green. **(c)** Heat map showing hierarchical

Euclidean (average) clustering of licensed MSC secretomes (x) and K-means clustering (n=6) of secreted proteins (y) based on intensity. Higher protein intensity is indicated in red and lower in blue. **(d)** Top 10 overrepresented GO BP terms for each K-means cluster of licensed MSC secretomes were plotted as horizontal bar graphs. Bar length indicates fold enrichment, colour indicates significance (-log10 FDR) as per the legend.

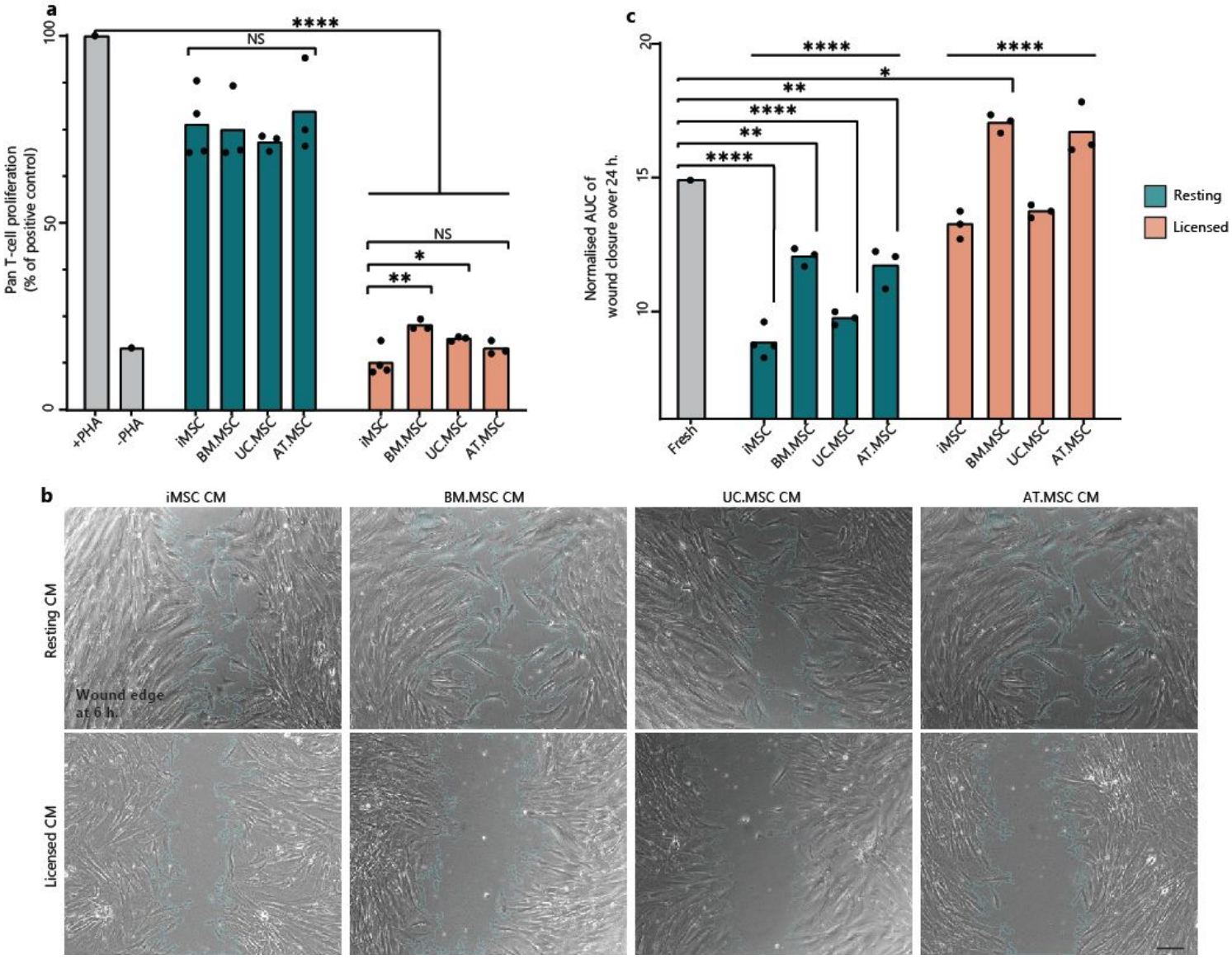

Figure 6

Functional response to MSC CM. (a) Bar graph showing the proliferation of activated pan T-cells treated with resting or licensed CM from different MSC sources (1:2 ratio) in comparison to activated (+PHA) or inactivated (-PHA) (+/- 5ug/mL PHA) controls. Data is plotted as the average (n=3 technical replicates) for each MSC line under resting (teal) or licensed (coral) conditions. **(b)**Representative images of wounded fibroblast cultures at 6 h in resting or licensed CM from different MSC sources. Scale bar is 200 µm. Wound edge is outlined in teal using ImageJ Wound Healing Analysis plugin. **(c)** Bar graph showing the area under the curve (AUC) of wound size in a fibroblast monolayer treated with resting or licensed

CM from different MSC sources in comparison to fresh media control (grey). Data is plotted as the average (n=3 technical replicates) for each MSC line under resting (teal) or licensed (coral) conditions with. Statistical significance was calculated by one-way ANOVA (*$p < 0.0332$, **$p < 0.0021$, ***$p < 0.0002$, ****$p < 0.0001$) against fresh media control (n=3 technical replicates).

Supplementary Files

This is a list of supplementary files associated with this preprint. Click to download.

- SupplementaryMaterialA.xlsx
- supplementaryfigures.pdf